Characterization of vehicle-to-vehicle channels in various scenarios

Student: Anna Roma
Supervisor: Laura Bernadó
Teacher: Christoph Mecklenbräuker and Thomas Zemen

Contents

List of Figures

List of Tables

1 List of abbreviation

VANET Vehicular ad hoc network

MANET Mobile ad hoc network

V2V Vehicular-to-Vehicular

WAVE Wireless Access in Vehicular Environments

ITS Intelligent Transportation Systems

OFDM Orthogonal Frequency Division Multiplexing

DSRC Dedicated Short Range Communication

I2V Infrastructure-to-Vehicle

MIMO Infrastructure-to-Vehicle

PDP Power Delay Profile

TX Transmitter

RX Receiver

LOS Line of Sight

ISI Inter Symbol Interference

ICI Inter Carrier Interference

DSD Doppler Spectrum Density

ULA Antenna linear array

ACF Auto Correlation Function

WSS Wide Sense Stationary

US Uncorrelated Scatterers

MPC Multi Path Component

GSCM Geometry-based stochastic model

LSF Local Scattering Function

GI Guard Time

MCD Multipath Component Distance

DBSAN Density-based spatial clustering of applications

2 Acknowledgements

I would like to offer my heartfelt thanks to Thomas Zemen for giving me the opportunity to be part of FTW, for his enthusiasm and for his extensive support during this thesis. I especially wish to thank him for helping during the whole procedure of this thesis, who always gave me the best hints and helps.

To my supervisor Christoph Mecklenbräuker for accepting to be my supervisor, for his ideas and advice have been guiding this thesis. But above all, for his time, patience, and understanding.

I would like offer my heartfelt thanks to my supervisor Laura for making this study possible. For her continued willing to teach me and help me in every step of my project, for her warmth and friendship to share concerns, successes and failures during the thesis, for teaching me to face the obstacles with joy, for supporting me in moments of anguish and despair. But above all, for being my family in Vienna and for becoming an essential friend in my life. Laura, it has been an honor to know you and work with you.

To Signal Processing department to pay attention in my presentations, for their interest in my thesis and for their valuable criticism in discussing the results of this work.

Furthermore, I wish to thank all friends and fellow students accompanying me during my years of study, who during these years have become my step-family.

Also I would like to thank my family and especially my parents for their support, enabling this study I have chosen and also helping me afford this marvelous time in Vienna.

3 Introduction

Vehicular ad hoc networks (VANET) are an important part for efficient future intelligent traffic management systems (ITS). Such a VANET includes vehicle-to-vehicle (V2V) as well as vehicle-to-infrastructure (V2I) communication links. A VANET needs robust transceiver algorithms, multiple-access control (MAC) and routing protocols to allow for a stable and economic operation. Reliable data communication for safety as well as user applications to mobile nodes at high velocity must be provided with strictly upper bounded delays.

In order to understand what a VANET is, we first introduce the definition of a MANET. The mobile ad hoc networks (MANETs) is a distributed network where the devices are connected through wireless links. Its topology is dynamic as nodes can move randomly, where every one of them can work as a host or a router as there is no infrastructure in the network.

A special type of MANET is the vehicular ad hoc network. The idea is to provide communication between different road vehicles, where each of them, equipped with a VANET device, will be a node of the mobile network. These ad hoc networks is characterized by vehicular velocities of each node and some fixed infrastructures in the form of access points along roads or motorways.

The major driving force for VANETs, is the goal to decrease the number of accidents and casualties on the roads significantly. Considering that most of the accidents are caused by human errors, such as slow reaction time, it seems obvious that being warned beforehand would help to avoid them. This kind of applications will be especially useful in:

Accident warning: At common driving velocities within one second a car passes a distances of 20 to 30 meters. Therefore, increasing as much as possible the reaction time can be very valuable. Safety applications could be useful to warn the drivers of an accident that occurred further down on the same road. Or furthermore, there could be a warning when the distance between two vehicles decreases critically, avoiding directly the first collision.

Intersections: At intersections the driver should be more careful as flows of traffic are crossing. In 2008, only in the state of Alabama, 178 fatal accidents occurred in intersections, according to the US- Department of Transportation. The number of such accidents would decrease if safety applications could warn the drivers of upcoming vehicles.

Traffic jams: As a result of the above, the number of traffic jams would also decrease. Safety applications could, apart from helping to avoid the accidents, choose an alternative routing, preventing that way, road congestion. And again, the effect would be drivers that are less frustrated by traffic jams and therefore, more concentrated, contributing again to avoid accidents.

Cellular channel models used until now are not suitable for vehicular communications. In order to derive a channel model that well represents the propagation characteristics of vehicular channels, the underlying fading process has to be well understood. Therefore, adequate measurement campaigns and posterior data analysis should be carried out in order to identify the main characteristics of this kind of radio channel.

4 Problem statement

In this section we start by defining briefly 802.11p communication system, and then explain the related work in this topic and finally present our objectives.

4.1 802.11p short description

The 802.11 standard has been widely used in different experiments with vehicle to vehicle communications [1, 2], concretely the 802.11a, b, or g. Vehicular environments impose a set of new requirements on IEEE 802.11. Hence, the IEEE approved a new amendment, IEEE 802.11p, also called Wireless Access in Vehicular Environments (WAVE). This amend- ment defines enhancements to 802.11 required to support intelligent transportation systems (ITS) applications.

The physical layer of 802.11p is very similar to the one of IEEE 802.11a [3]. The major difference between both technologies is that the sampling time is doubled (and the bandwidth is reduced by one half from)20 to 10MHz such that the inter-symbol interference caused by multipath is decreased. Due to the bandwidth reduction 20 to 10MHz the data throughput range reduces from 6 ... 54 Mb/s to 3 ... 27 Mb/s. By using the multihop technique, WAVE has a transmission range between 300 and 1000 meters. The modulation format for 802.11p is orthogonal frequency division multiplexing (OFDM) similar as for 802.11a.

1999 in the United States, the U.S. Federal Communication Commission allocated 75MHz of Dedicated Short Range Communications (DSRC) spectrum at 5.9 GHz to be used exclusively for V2V and infrastructure-to-vehicle (I2V) communications [4, 5].

As shown in Fig. **??**, the DSRC spectrum is structured into seven channels of 10 MHz bandwidth each. Channel 178 is the control channel, which is restricted to safety communications only. The two channels at the ends of the spectrum band are reserved for special uses. The rest are service channels available for both safety and non-safety usages.

Similar efforts to set spectrum aside for vehicular usage are taking place in other parts of the world. The European committee, for example, has dedicated a frequency band for safety-related ITS with 30 MHz bandwidth at 5875-5905 MHz.

4.2 Related work

Here, we try to give an overview of work already done. So far only taken into account in V2V communications the scattering identification field.

In order to design efficient V2V systems, an understanding of realistic V2V propagation channels is required. Several measurement campaigns have been conducted in recent years to study the vehicular radio channel. The FTW was involved in two of them.

One of the first measurement campaigns was carried out in Lund in 2007. The measurements were taken in three different scenarios, trying to represent three of the "usual" V2V communication situations: an urban scenario, a rural scenario and on a highway. Each car was equipped with a 4 patch-element circular antenna array, allowing for a 4x4 multiple-input multiple-output (MIMO) measurements [6]. The carrier frequency was chosen to be at 5.2 GHz with a bandwidth of 240 MHz. The collected data comprised three different V2V set-ups: 1) Cars driving in the same direction, 2) cars driving in the opposite direction, and 3) V2I measurements. The authors analyzed the vehicular radio channel by visual inspection from the Power Delay Profile (PDP) and Delay-Doppler spectrum [7], [8]. When the cars are driving in opposite directions the Doppler shift is higher, because of the higher relative speeds between transmitter (TX) and

receiver (RX). The authors in [7] analyzed the origin of the observed paths in the delay-Doppler spectrum, and their time dependency. Using the same measurement campaign data, the time varying rms delay spread and excess delay were analyzed in [8], in relation to the PDP for a highway scenario. First results tackling the issue of the non-stationarity in the fading processes for vehicular communications were presented in [17], [9] and [10]. Additionally, they found several path with a constant delay and zero Doppler over time [7] as well as multiply reflected paths with very high Doppler shifts. Another studies about the same campaign [8], is focused on estimate different channel parameters as rms delay spread and excess delay from the PDP in a highway scenario. They diffuse paths with small delays aroun the line of sight (LOS) where investigated in [8]

Based on the 2007 campaign, another measurement campaign was organized in June 2009 called DRIVEWAY to find new results. In this case the center frequency was 5.6 GHz and also linear patch-type array-MIMO antennas were used and the scenarios risk situations were chosen. In [11] the PDP and the Doppler spectrum density (DSD) were evaluated in two different scenarios. As done in previous work, they continued analyzing the different scattering contributions in these functions from visual inspection. The authors found that the reflections were produced by big metallic surfaces, they distinguished between mobile (trucks, other cars) or static contributions (traffic signs, bridges, buildings).

Other measurements campaigns have been conducted in recent years such as Guillermo Acosta in Atlanta [12, 13], Indranil Sen in Athens [14], P. Paschalidis [15] or Lin Cheng in Pittsburgh [16].

4.3 Objectives of the master thesis

The main objective of this master thesis is to characterize the time-varying parameters of the vehicular radio channel in various scenarios. We focus in the following:

- 1. Time-varying relevant contributing objects
- 2. Delay and Doppler rms spreads: In order to characterize the radio channel, we have a look at its statistical properties. The parameters are useful to avoid the Inter Symbol Interference (ISI) and the Inter Carrier Interference (ICI).
- 3. Stationarity time: for how long we can consider that the statistical description of the fading process in the channel remains constant in time.

5 Data description - DRIVEWAY'09

In this thesis we use the radio channel measurements collected in the DRIVEWAY campaign in June 2009. In [11], more information about the DRIVEWAY campaign can be found. The measurements were carried out in the cities of Lund and Malmö, both in Sweden.

Hence, it will be useful to know the equipment used to get the measurements and the different parameters that were chosen for the occasion. We must not forget to describe the scenarios which will help us to understand the results.

5.1 Measurement Equipment

The RUSK LUND channel sounder was used for carrying out the channel measurements, and it performs MIMO measurements based on the "switched-array" principle.

The transmitter and receiver are equipped with 4 antenna each, resulting in a total number of 16 individual measured links. The antenna module consists of $N = 4$ identical elements in a uniform linear array (ULA) configuration featuring interelement spacings of $\lambda/2$ [6]. The antenna elements are based on the concept of a circular patch which is driven in a higher operational mode, thus leading a terrestrial radiation patter. Following the conventional mounting position for roof-top antennas on the rear part of the vehicle, Volkswagen Touran measurements vehicles were equipped with the antenna modules. The ULA orientation was chosen perpendicular to driving direction.

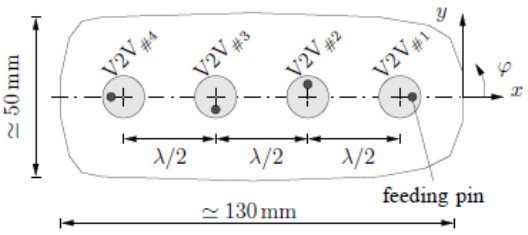

(d) Block diagram of the ULA including $N = 45$ elements

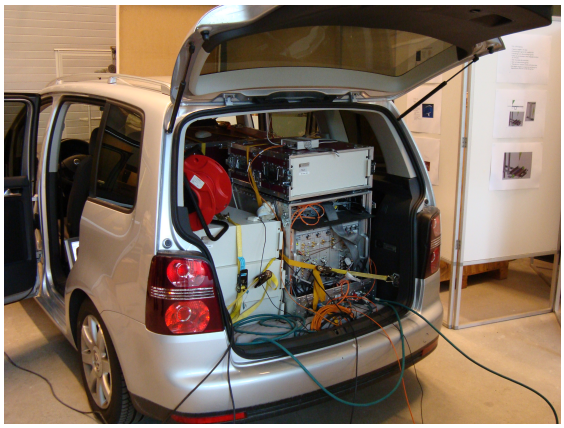

(e) Reciver part of the channel sounder mounted in the truck of one of the measurement cars

Figure 1: Measurement equipment

5.2 Measurement Parameters

The measurements were taken with a large bandwidth of 240 MHz at a center frquency of 5.6 GHz. This center frequency is very close to the allocated 5.9 GHz, the frequency band for ITS in Europe. For that reason, we don't expect a different behavior. The measurement setup of the channel sounder is summarized in the next table:

Table 1: Measurement Parameter setting.

Parameters	
Carrier frequency [GHz]:	5.6
Measurement bandwidth [MHz]:	240
Transmit power [dBm]:	27
Testsignal length [μs]:	3.2
Number of snapshots:	32500
Number of Tx elements:	4
Number of Rx elements:	4
Snapshot time [μs]:	102.4
Snapshot repetition time [μs]:	307.2
Recording time [s]:	10

5.3 Measurement Scenario

In this section we present the various scenarios we will focus our work. The scenarios and situations were chosen based on the importance for safety-related ITS on applications such as collision avoidance, emergency vehicle warning, pre-crash sensing warning, hazardous location notification, wrong way driving warning, co-operative merging assistance, traffic condition warning, stationary vehicle warning, slow vehicle warning, lane change assistance, co-operative forward collision warning and overtaking vehicle warning.

We must describe the meaning of scenario and experiment. We call "scenario" each risk situation we are studying, and we speak about an "experiment" each time we take measurements from one scenario.

In the following we will describe the different scenarios in a more detailed manner.

5.3.1 Scenario 1: Road Crossing

This scenario consists of a conventional road crossing in rural and urban environments. The measurement vehicles are approaching the crossing from different directions with different velocities v_{TX} and v_{RX}. In this scenario we distinguish four sub-scenarios where the data was taken. The first environment is an open area road crossing. In the other three environments there is obstructed LOS at the beginning of the measurements. Besides the obstructed LOS there is either an open surrounding area or surrounding buildings, where in the latter case a single lane and multiple lane scenario are considered.

Sub-scenarios:

- Scenario 1.1- Open Area Rural: 3 experiments

- Scenario 1.2- Obstructed LOS, otherwise open surroundings (suburban): 11 experiments
- Scenario 1.3- Obstructed LOS, otherwise surroundings - single lane (urban): 5 experiments
- Scenario 1.4- Obstructed LOS and surroundings buildings - multiple lanes (urban): 5 experiments

Possible Applications:

- Emergency vehicle warning
- Intersection collision warning
- Pre-crash sensing warning

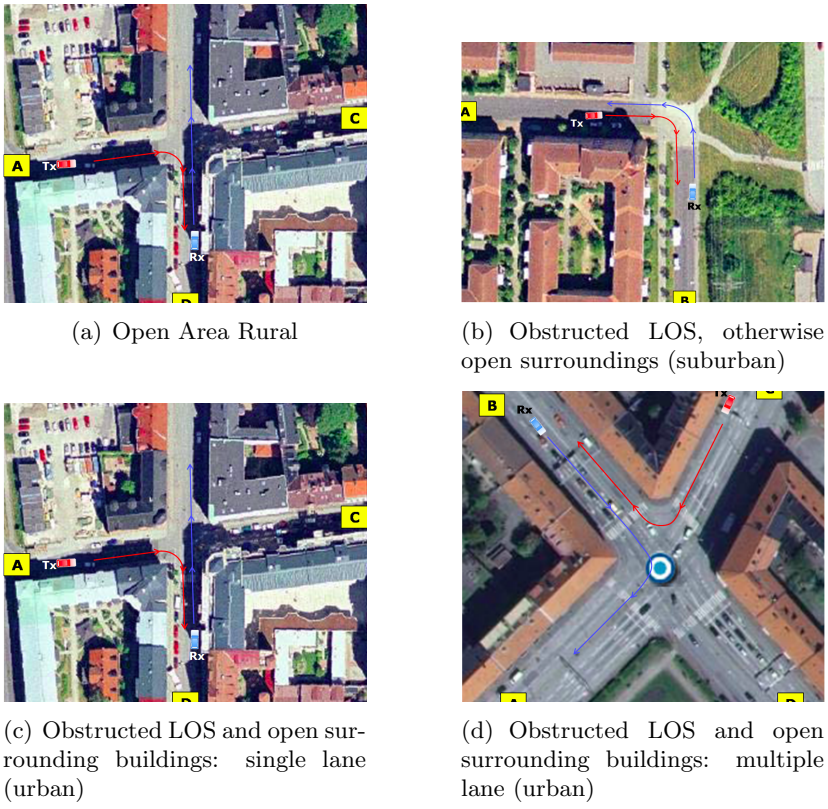

(a) Open Area Rural

(b) Obstructed LOS, otherwise open surroundings (suburban)

(c) Obstructed LOS and open surrounding buildings: single lane (urban)

(d) Obstructed LOS and open surrounding buildings: multiple lane (urban)

Figure 2: Measurement location for scenario 1

5.3.2 Scenario 2: General LOS obstruction

This scenario investigates the influence of LOS obstruction on the propagation. TX and RX are driving in the same direction on the highway with velocities v_{TX} and v_{RX}, respectively. In this situation, one truck is blocking the LOS.

Sub-scenarios:

- Scenario 2.1- General LOS obstruction: 12 experiments

Possible Applications:

- Hazardous location notification

(a) Measurement schematics (b) Measurement location

Figure 3: Measurement location for scenario 2

5.3.3 Scenario 3: Merging lanes

This scenario is characterized by a certain angle between intersecting roads. The Rx car is driving on the highway and the TX car is entering the highway on a partly obstructed entrance ramp.

Sub-scenarios:

- Scenario 3.1- Merging lanes: 9 experiments

Possible Applications:

- Wrong way driving warning
- Co-operative merging assistance

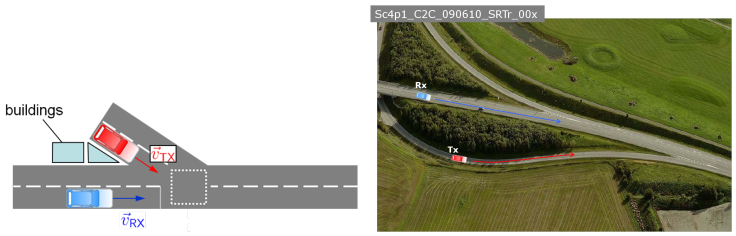

(a) Measurement schematics (b) Measurement location

Figure 4: Measurement location for scenario 3

5.3.4 Scenario 4: Traffic congestion

Different situations in a traffic congestion are considered. Both cars are stuck in the traffic congestion, and one car is approaching the traffic congestion, where the other car is stuck.

Sub-scenarios:

- Scenario 4.1- Traffic congestion - Slow traffic: 11 experiments
- Scenario 4.2- Traffic congestion - Approaching traffic jam: 7 experiments

Possible Applications:

- Traffic condition warning

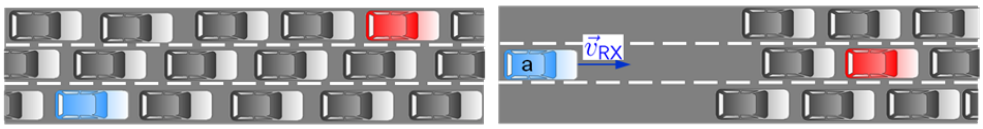

(a) Measurement schematics for scenario 4.1 (b) Measurement schematics for scanario 4.2

(c) Picture while on-going measurement

Figure 5: Measurement locations for scenario 4

5.3.5 Scenario 5: In-tunnel

The measurements are carried out on the Oresund tunnel, where both cars are driving in the same direction with different distances and varying number of cars between them.

Sub-scenario:

- Scenario 5.1- In-tunnel: 7 experiments

Possible Applications:

- Emergency electronic brake lights
- Slow vehicle warning
- Lane change assistance
- Co-operative forward collision warning

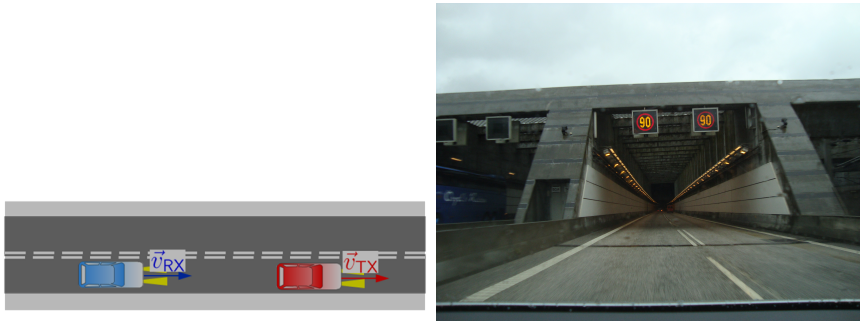

(a) Measurement schematics (b) Measurement location: In-tunnel

Figure 6: Measurement location for scenario 5

5.3.6 Scenario 6: On bridge

The measurements for this scenario were taken on the bridge before the Oresund tunnel, which is held over the sea. The two cars drive in the same direction with a separation of about 150 m. The bridge is composed by big metallic structures, equidistantly spaced.

Sub-scenario:

- Scenario 6.1- In-tunnel: 3 experiments

Possible Applications:

- Overtaking vehicle warning
- Emergy vehicle warning
- Slow vehicle warning

(a) Measurement location: Bridge (b) Measurement location: Bridge

Figure 7: Measurement location for scenario 6

6 Concepts definition - Theory

6.1 Radio channel description

6.1.1 The wireless channel

In mobile communications, the data transference between transmitter and receiver occurs through radio waves. The communication path joining TX and RX when there are no obstacles in between is called line-of-sight. In addition to the LOS path, delayed copies of the sent signal reach the RX. These are the result of reflections or diffractions on buildings, mountains or other objects. Each one of these paths has different amplitude, delay, direction of departure from the TX and arrival to the RX, and different phase shifts.The different propagation mechanisms influence pathloss and fading models differently. However, for convenience we refer to all these distorting mechanisms as "scattering".

Figure 8 shows a typical set-up of a communication between a fixed TX and a mobile RX. There we can see which objects are causing the multipath.

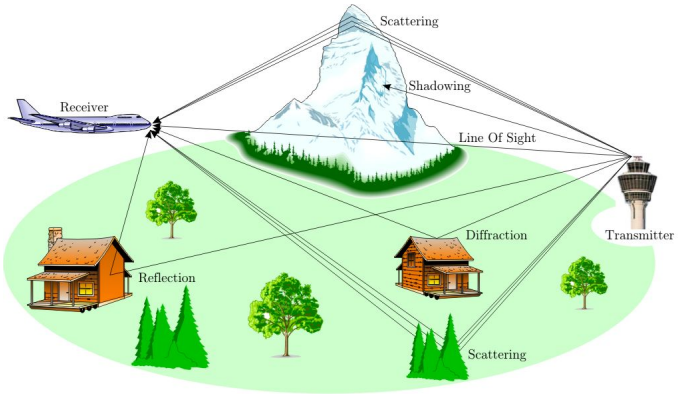

Figure 8: Multipath propagation

Pathloss and fading

Path loss includes all of the lossy effects associated with distance and the interaction of the propagating wave with the objects in the environment between the antennas.

Path loss may be due to many effects, such as free-space loss, refraction, diffraction, reflection, and absorption. Path loss is also influenced by terrain contours, environment (urban or rural, vegetation), propagation medium (dry or moist air), the distance between the transmitter and the receiver, and the height and location of antennas.

In addition to pathloss, the received signal exhibits fluctuations in signal level called fading. Fluctuation in signal level is typically composed of two multiplicative components: large-scale fading and small-scale fading:

- large-scale fading: Represents the long term variation of the received signal power level and it is caused by shadowing effects. Shadowing is when the received power is attenuated because of the wave is blocked through some obstacle. See Fig. 8. The power keeps attenuated until TX or RX leave the obstacle behind.

- small-scale fading: Represents the short term variation of the received signal power level and it refers to the rapid fluctuations of the received signal in space, time and frequency. It is caused by the signal scattering off objects between TX and RX.

Figure 9, shows clearly the three phenomenons, in black the pathloss, built on it, the large-scale fluctuations, in red, and finally in blue the small-scale fading.

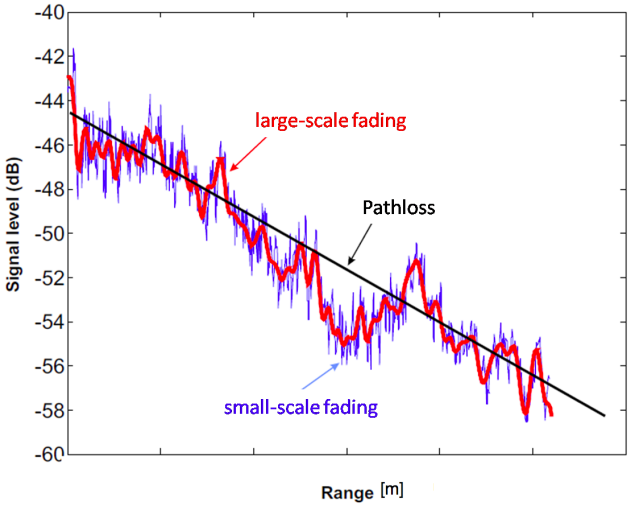

Figure 9: Signal power fluctuation vs range in wireless channels

6.1.2 The WSSUS model

In mobile communications, the statistical characterization of the radio channel is complicated because the correlation functions depend on four variables:

$$\begin{aligned} R_h(t, t+\Delta t, \tau, \tau') \\ R_H(t, t+\Delta t, f, f+\Delta f) \\ R_S(\upsilon, \upsilon', \tau, \tau') \\ R_B(\upsilon, \upsilon', f, f+\Delta f), \end{aligned} \tag{1}$$

where the variables t, f, τ, and ν are time, frequency, delay and Doppler shift respectively.

However, it is possible to simplify the correlation functions by considering valid two assumptions on the random process, which will be described in the following sections.

WSS assumption

A random process whose Auto Correlation Function (ACF) only depends on the time difference $t - t'$ and not on the two variables t, t' separately is assumed to be Wide Sense Stationary (WSS). This is, the statistical properties of the channel do not change with time. The ACF will be,

$$R_h(t, t', \tau, \tau') = R_h(\Delta t, \tau, \tau').$$

We obtain consequently uncorrelation in the transformed as,

$$R_S(\upsilon, \upsilon', \tau, \tau') = P_S(\upsilon, \tau, \tau')\delta(\upsilon - \upsilon')$$

$$R_B(\upsilon, \upsilon', f, f') = P_B(\upsilon, f, f')\delta(\upsilon - \upsilon').$$

So, WSS defines contributions with different Doppler shifts are uncorrelated.

US assumption

When contributions with different delays are uncorrelated, the random process is assumed to be Uncorrelated Scatterers (US). In this case, the time-delay and Doppler-delay ACFs could be simplified resulting,

$$R_h(t, t', \tau, \tau') = P_h(t, t', \tau,)\delta(\tau - \tau')$$

$$R_S(\upsilon, \upsilon', \tau, \tau') = P_S(\upsilon, \upsilon', \tau)\delta(\tau - \tau').$$

We assume US when the phase of an Multi Path Component (MPC) does not contain any information about the phase of another MPC with a difference delay.

Similarly as for the WSS case, the ACFs are not dependent on the absolute frequency, only on the frequency difference as,

$$R_H(t, t', f, f + \Delta f) = R_H(t, t', \Delta f).$$

The WSSUS assumption

The WSSUS assumption has become usual for characterizing random fading processes. The ACFs in (1) could be simplified to a two-variable dependent functions by assuming the fading process to be WSSUS resulting as,

$$\begin{aligned} R_h(t, t + \Delta t, \tau, \tau') &= P_h(\Delta t, \upsilon)\delta(\tau - \tau') \\ R_H(t, t + \Delta t, f, f + \Delta f) &= R_H(\Delta t, \Delta f) \\ R_S(\upsilon, \upsilon', \tau, \tau') &= P_S(\upsilon, \tau)\delta(\upsilon - \upsilon')\delta(\tau - \tau') \\ R_B(\upsilon, \upsilon', f, f + \Delta f) &= P_B(\upsilon, \Delta f)\delta(\upsilon - \upsilon'). \end{aligned}$$

Locally WSSUS assumption

Unfortunately, the WSSUS assumptions is not valid for vehicular-to-vehicular radio channels. The WSS assumption is not fulfilled because the second order statistics of the fading process change over time. Moreover, the contributions with different delays can be correlated, when they come from the same object, thus the US assumption is also not fulfilled. In [17], the authors found that V2V channels violate the wide-sense stationary much stronger than the US assumption.

In order to characterize such processes, one can assume that the WSSUS property holds in time-frequency limited regions [18]. The length of these stationarity regions is still under investigation. The maximum time during which the WSSUS assumption is valid is called stationarity time. First results in this direction were presented in [9], where a stationarity time in a highway where the vehicles are driving in opposite directions was found to have a mean value of 23 ms. Whereas if vehicles are driving in the same direction on an urban street, is 1479 ms.

6.1.3 Modeling Approaches

For the design, simulation and planning of wireless system we need models for the propagation channels. Several models had been studied [19], but in general, there are three fundamental approaches to channel modeling:

- Ray tracing (Deterministic): Realistic simulation of the V2V propagation channel. The model requires the definition of the location, shape, and electromagnetic properties of objects. At the same time, however, it needs intensive computations.
- Stochastic: it provides the statistics of the power received with a certain delay, Doppler shift, angle-of-arrival etc. The most important stochastic channel model is the tapped-delay-line model, which is based on the WSSUS assumption.
- Geometry-based stochastic model (GSCM) [20]: it is well suited for vehicular communications, since it takes into account the non-stationarity of the fading process. A more detailed description of this model is given in the next section.

6.1.4 Geometry-based stochastic channel model

The GSCM consists of using randomly placed scatterers around TX and RX according to a statistical distribution. Then, the signal contributions of the scatterers are determined from simplified ray tracing, and finally the total signal is summed up at the receiver.

The GSCM makes a distinction between discrete and diffuse scattering:

- Discrete scatterers: cars, houses, road signs, and other strong scattering points along the measurement route.
- Diffuse scatterers are the sides of the measurement route.

In [20], the authors distinguish between three types of scatterers: mobile discrete, static discrete and diffuse. The total channel impulse response

$$h(t,\tau) = h_{LOS}(t,\tau) + \sum_{p=1}^{P} h_{MD}(t,\tau_p) + \sum_{q=1}^{Q} h_{SD}(t,\tau_q) + \sum_{r=1}^{R} h_{DI}(t,\tau_r)$$

is the sum of the all contributions:

LOS: Line-of-sight between TX and RX,

Mobile-discrete scatterers: discrete components stemming from reflections off P mobile scatterers,

Static-discrete scatterers: discrete components stemming from reflections off Q static scatterers, and

diffuse scatterers: diffuse components from reflections off R diffuse scatterers.

Figure 6.1.4 depics a typical power delay profile for a situation with time-varying obstructed LOS between TX and RX, we can observe the different contributions listed previously.

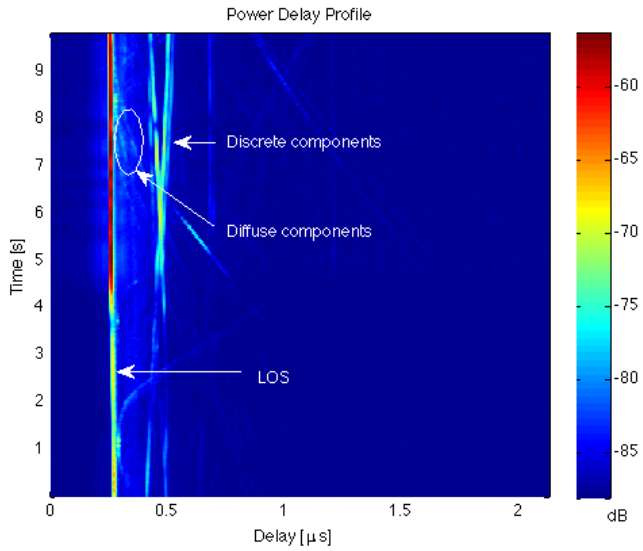

Figure 10: Time-varying power-delay profile for a typical obstructed LOS highway scenario.

6.2 Measured channel

6.2.1 Impulse response

As mentioned previously, the information in wireless communication is received by different path where each contribution has a different attenuation and delay. The contributions can be constructive and destructive and they gives the impulse response.

Next we present the sampled channel transfer function of a linear time-variant channel $\mathbf{H}$

$$L_{\mathbf{H}}[m,q] = L_{\mathbf{H}}(mt_{\text{rep}}, q/(N\Delta\tau)) \tag{2}$$

is measured by the channel sounder and stored over a duration of $t_{\text{rec}} = 10\,\text{s}$, with time index $m \in \{0 \ldots S'-1\}$ and frequency index $q \in \{-(N'-1)/2 \ldots (N'-1)/2\}$. We obtain the complex sampled channel impulse response

$$h[m,n] = h(mt_{\text{rep}}, n\Delta\tau) \tag{3}$$

by means of an inverse Fourier transform using a Hanning windowing function. No significant signal components were measured for delays larger than $1\,\mu\text{s}$, hence we consider only the first $N = 256$ delay samples, $n \in \{0, \ldots, N-1\}$. The time index m was limited to a segment with time duration of $t_{\text{seg}} = 2\,\text{s}$ for all three scenarios, $m \in \{0, \ldots, S-1\}$ with $S = 6500 = S't_{\text{seg}}/t_{\text{rec}}$.

6.3 Local scattering function

The Local Scattering Function (LSF) is the distrubution of the power in delay and Doppler shift domain as you can see in Fig. 11 As we comment before in 6.1.2, the WSSUS assumption is not valid for a vehicular radio channels, especially for high speed. We use the concept of a LSF which is defined for non-WSSUS channels in [18] for continuous time as

$$\mathcal{C}_{\mathbf{H}}(t,f;\tau,\nu) = \int_{-\infty}^{\infty}\int_{-\infty}^{\infty} R_h(t,\tau;\Delta t,\Delta\tau) \times e^{-j2\pi(\nu\Delta t + f\Delta\tau)} d\Delta t\, d\Delta\tau\,,$$

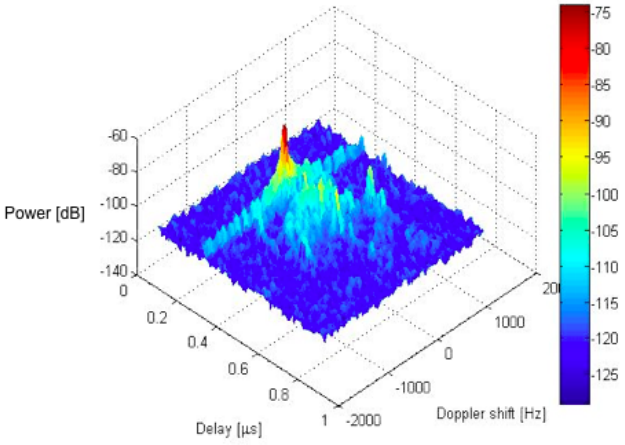

Figure 11: LSF for a time instance

where

$$R_h(t,\tau;\Delta t,\Delta\tau) = Eh(t,\tau+\Delta\tau)h^*(t-\Delta t,\tau)$$

As explained in [18] the LSF is not guaranteed to be positive and furthermore depends on the whole correlation function $R_h(t,\tau;\Delta t,\Delta\tau)$.

The interpretation that we can find in [9], allows to obtain a practical estimation method [21] which we will use for our vehicular channel measurements. From now on we will omit the explicit dependence of $\mathcal{C}_{\mathbf{H}}$ on f considering the dependence of the LSF on t only. We use a discrete time implementation of the scattering function estimator described in [21].

Finally, the multi-window spectrogram is computed according to

$$\mathcal{C}_{\mathbf{H}}^{(\Phi)}[m;n,p] = \frac{1}{IJMN}\sum_{k=0}^{K-1}\left|\mathcal{H}^{(\vec{G}_k)}[m;n,p]\right|^2$$

with $n \in \{0,\ldots,N-1\}$ and $p \in \{-M/2,\ldots M/2-1\}$ where $M = 128$ samples and $N = 512$ samples,

$$\mathcal{H}^{(G_k)}[m;n,p] = \sum_{m'=-M/2}^{M/2-1}\sum_{q'=-N/2}^{N/2-1} L_{\mathbf{H}}[m',q'] \times L_{G_k}[m'-m,q']e^{-\jmath 2\pi(pm'-nq')}\,.$$

Note that $L_{\mathbf{H}}[m,q] = L_{\mathbf{H}}(mt_{\text{rep}}, \frac{q}{N\Delta\tau})$ and $\mathcal{C}_{\mathbf{H}}^{(\Phi)}[m;n,p] = \mathcal{C}_{\mathbf{H}}^{(\Phi)}(mt_{\text{rep}};n\Delta\tau, \frac{p}{Mt_{\text{rep}}})$.

6.4 Power delay profile and Doppler spectral density

The PDP, also called the multipath intensity profile, gives the average power at the multipath channel as a function of time delay. The time delay is the difference in travel time between multipath arrivals. We defined the abscissa and ordinate in units of time, being delay [μs] and time [s] respectively. It is easily measured empirically and can be used to extract certain channel's parameters such as the delay spread. Commonly it is assumed that PDP and DSD are time invariant, however, in vehicular channels they happen to be time varying. Therefore the PDP and DSD are defined as time-varying functions and they are based in LSF [19].

$$PDP(t,\tau) = \int LSF(t;\tau,\upsilon)d\upsilon.$$

Analogously, but with the Doppler variable is calculated the DSD,

$$DSD(t, \upsilon) = \int LSF(t; \tau, \upsilon) d\tau.$$

6.5 Time-varying channel characterization

To compare different multipath channels and to develop some general design guidelines for wireless system is important estimate some channel parameters witch are derived from the PDP and DSD.

The channel is highly time-varying, and the channel parameters are changing quickly. In order to properly characterize the radio channel parameters, we need to study their time variability. Radio channel parameters such as delay and Doppler spreads are commonly used for system design and channel modeling.

Due to the already mentioned time variability of the channel, it is also important to characterize the time over which the channel can be considered stationarity. For all these reasons, the work in this master thesis is going to be focused on delay spread, Doppler spread and the stationarity time.

6.5.1 Data pre-processing

In order to obtain non misleading results, we preprocess the data before estimating the channel parameters. We do that by setting two thresholds on the PDP ans DSD, described in the following.

Noise thresholding

In a perfect channel affected by multipath, the channel impulse response of a noise-less wireless channel affected by multipath looks like a series of pulses. In practice, the channel is not ideal and it seems like Fig. 12. Usually is corrupted by noise, the last contributions

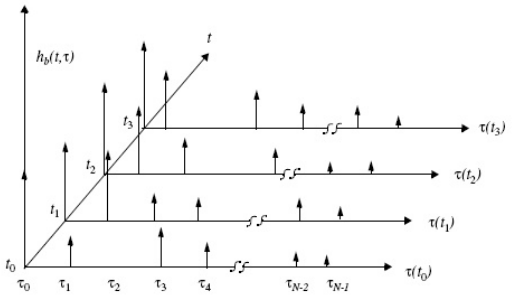

Figure 12: An example of the time-varying impulse response model for a multipath

of the impulse response is just noise. It is important that rms delay spread and rms Doppler spread are not affected by the noise.

We take care of that by setting a threshold, which is defined 5 dB adove the noise power. All the components bellow that threshold are set to zero.

Receiver sensitivity thresholding

In this case, we set to 0 all the components which are below the maximum value at a given time instantanius 40 dB. This threshold is useful for receiver sensitivity. The sensitivity

is the minimum input signal that allows to output a signal/noise ratio default (usually ¿ 20 dB)

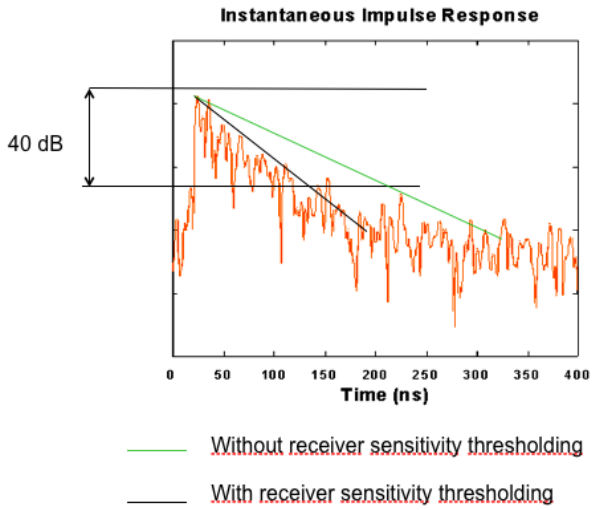

Figure 13: Receiver sensitivity thresholding

Next figure shows the PDP and the rms delay spread in road crossing scenario with the thresholds that we have already presented. We compare the PDP with and without threshold and we realize that the contributions from the noise has already disappear when we use threshold. This makes the rms delay spread more reliable than without threshold.

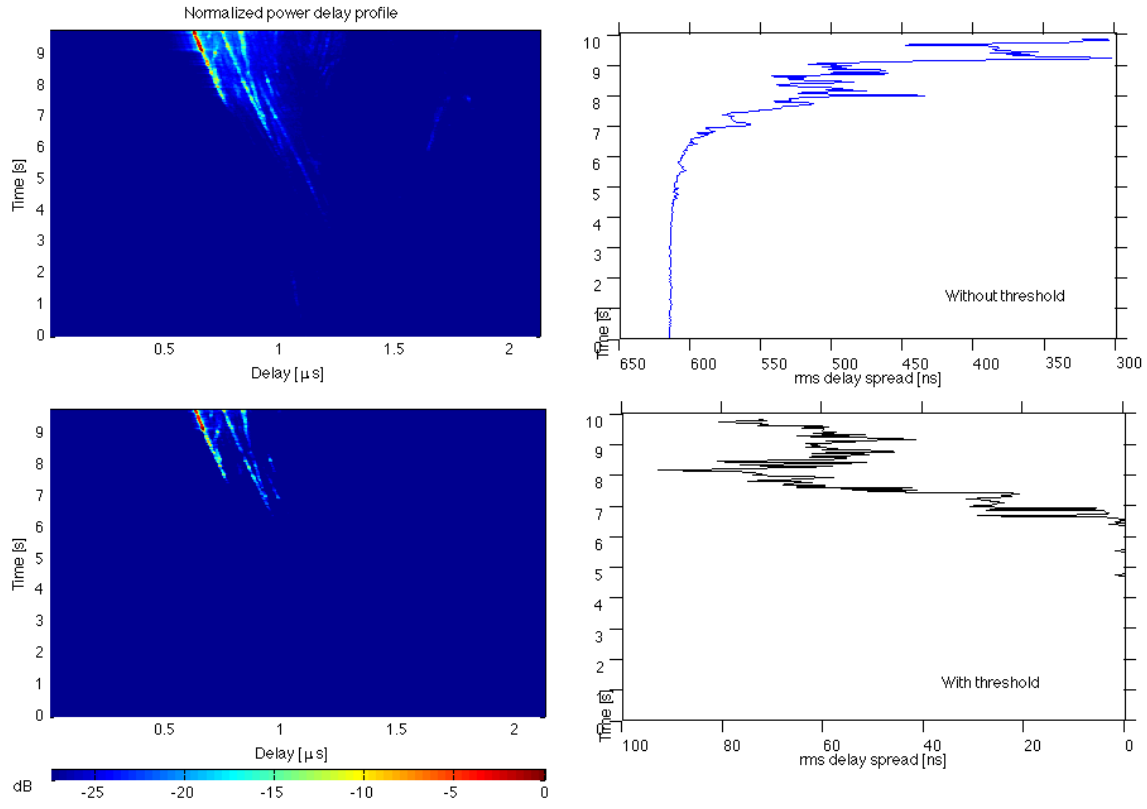

Figure 14: PDP and rms delay spread in road crossing scenario with and without threshold

6.5.2 rms delay and Doppler spreads

In order to characterize the radio channel, we have a look at its statistical properties. As mentioned before, vehicular channels are locally WSSUS and therefore the statistical parameters are also locally defined.

The standard 802.11p will be used for vehicular communications and it utilizes with OFDM communication system. A guard time (GI), is attached to each data OFDM symbol in order to eliminate the ISI introduced by the multipath propagation. The GI has to be larger than the delay spread to prevent ISI, $GI > \sigma_{rms,\tau}$.

On the other hand, if the rms Doppler spread is larger than 10 of the sub-carrier separation, then we will observe ICI.

In that sense, we will evaluate time-varying delay and Doppler spread.

Delay spread and coherence bandwidth

The rms delay spread is defined as the delay span between the first received peak and when it has delayed 1/e.

In a multipath propagation environment, several delayed scaled versions of the transmitted signal arrive at the receiver. The delay separation between paths increases exponentially with path delay, and the path amplitudes also fall off exponentially with delay. The span of path delays is called the delay spread and it is the normalized second-order central moment of the PDP defined as [19]:

$$S_\tau(t) = \sqrt{\frac{\int_{-\infty}^{\infty} PDP(t,\tau)\tau^2\, d\tau}{P_m(t)} - T_m^2(t)}.$$

where PDP is the power delay profile:

$$PDP(\tau) = \int_{-\infty}^{+\infty} |h(t,\tau)|^2 dt, \tag{4}$$

P_m is the time-integrated power:

$$P_m = \int_{-\infty}^{+\infty} PDP(\tau) d\tau, \tag{5}$$

T_m is the mean delay:

$$T_m = \frac{\int_{-\infty}^{+\infty} PDP(\tau)\tau d\tau}{P_m}. \tag{6}$$

Typical values of rms delay spread in outdoor mobile radio channels are on the order of microseconds and in indoor radio channels around of nanoseconds.

The delay spread causes frequency selective fading which can be characterized in terms of coherence bandwidth, B_{coh}. The B_{coh} defines the frequency difference [19] that is required so that the correlation coefficient is smaller than a given threshold, normally typically used in the literature (-3dB below the maximum correlation bandwidth of the correlation function) and it is inversely proportional to the S_τ, thus:

$$B_{coh}(t) \approx \frac{1}{2\pi S_\tau(t)}. \tag{7}$$

Doppler spread and coherence time

We define the time-varying rms Doppler spread in a similar way as for the rms delay spread. In this case, it is the normalized second-order moment of the DSD [19],

$$S_\upsilon(t) = \sqrt{\frac{\int_{-\infty}^{\infty} DSD(t,\upsilon)\upsilon^2\, d\upsilon}{P_{B,m}(t)} - \upsilon_m^2(t)}.$$

$P_{B,m}$ is the doppler-integrated power:

$$P_{B,m} = \int_{-\infty}^{+\infty} DSD(\upsilon)d\upsilon, \tag{8}$$

υ_m is the mean Doppler:

$$\upsilon_m = \frac{\int_{-\infty}^{+\infty} DSD(\upsilon)\upsilon d\upsilon}{P_{B,m}}. \tag{9}$$

Time selective fading can be characterized by the coherence time, T_{coh}. The definition [19] of the T_{coh} is thus analogous to the B_{coh} and the T_{coh} is inversely proportional to the Doppler spread and can be approximated as

$$T_{coh}(t) \approx \frac{1}{2\pi S_\upsilon(t)}. \tag{10}$$

Methodology

We estimate the rms delay and Doppler spreads over time for the whole measurement run. As mentioned before, they change in time. We calculate then the mean of each experiment and the maximum value.

Bear in mind that sometimes we have no signal for a few seconds and we should not consider this part to calculate the average.

In order to characterize these values in a "per-scenario" basis, we calculate then the mean (and the maximum value) over all experiments, and present the results as a table at the end of the analysis of each individual scenario.

Identiability of wireless channels

The temporal variability of wireless channels has an impact on whether the channel can be identied (measured) in a unique way. For strongly time-varying channels, the requirements are:

- The repetition frequency T_{rep} has to be larger than the maximum excess delay of the channel τ_{max}
- The repetition frequency has to full $T_{rep} \leq 1/2\tau_{max}$.

Thus channels can be identied in an unambiguous way only if:

$$2\tau_{max}\upsilon_{max} \leq 1. \tag{11}$$

This equation is also known as the two-dimensional Nyquist criterion. A channel that fullls these requirements is known as underspread. If Eq.11 is not fullled, then the channel can only be identied by making specic assumptions - e.g., a certain parametric model. Fortunately, the majority of wireless channels are underspread.

6.5.3 Stationarity time

Another interesting parameter in a time-varying system is the stationarity time. It is the time that we assume that the process is stationary, and it is important basically because stationarity time is the maximum time during which the WSSUS assumption is valid.

Methodology

For estimating the stationarity time we use the collinearity metric, used already in previous publications for that purpose [17]. For comparing LSF at two different time instances. In fig. 15 we have an example of collinearity.

We defined the collinearity between LSF at two different time instances as,

$$R_{\mathcal{C}_\mathbf{H}}[m_1, m_2] = \frac{\vec{c}_\mathbf{H}[m_1]^T \vec{c}_\mathbf{H}[m_2]}{||\vec{c}_\mathbf{H}[m_1]||||\vec{c}_\mathbf{H}[m_2]||}$$

for two instances m_1 and m_2.

The collinearity is a bounded distance metric with 1 and0 as upper and lower bounds respectively. A collinearity of 1 means that the two compared LSF are equal (colour red). The more dissimilar they get, the closer to 0 the collinearity is (colour blue). Figure 15 shows the collinearity for merging lines scenario,

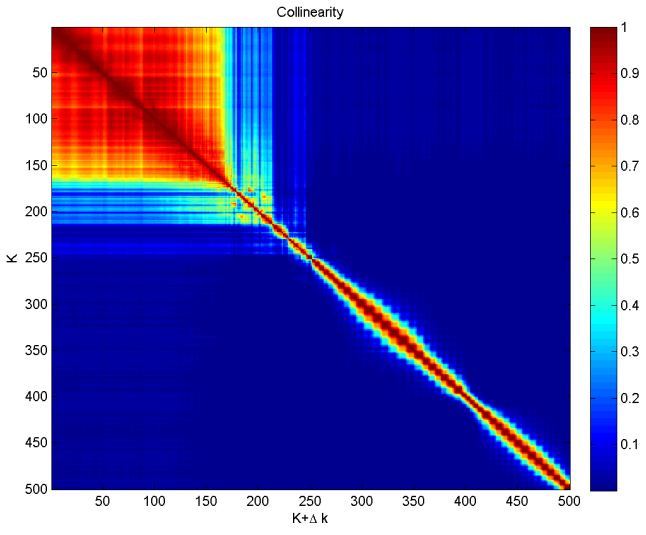

Figure 15: Collinearity

So, if we take a look in Fig. 15 we can realize that in the diagonal all the values are 1. This is because we compare one instance with itself, and they are very similar. The reddish square that we can see in the left upper corner of the graphic corresponds to a few seconds in the beginning of the measurement, where there is no signal yet, only noise. The statistics of noise at two different instances are very similar, therefore the outcome of the collinearity measures is close to 1.

For assuming that a process is stationary for a limited period of time, we should assure that the statistical description is more or less the same within that time interval. Here is were we use the collinearity metric for assessing similarity. We consider that the power spectral density is very similar when the collinearity measure is over 0.9. Therefore we set a threshold of 0.9 to the collinearity and measure at every time instance the time span over which the collinearity remains over 0.9, as shown in Fig. 16.

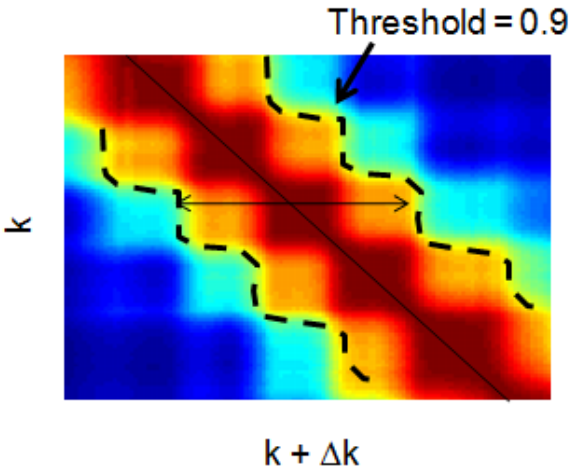

Figure 16: Area where we suppose that the process is stationarity

6.6 Cluster based time-varying scattering characterization

In this section, we explain why we are interested in identifying the relevant scatterers, and how we are going to do that by using clustering algorithms. First, we follow an heuristic approach by visual inspection of the PDP. A more accurate result can be obtained by introducing another domain in the analysis, the Doppler shift. Peak detection is needed in order to identify the relevant components. Finally, grouping the components in clusters, allows us to fully characterize the relevant scattering objects.

6.6.1 Concept

We start describing the first followed steps on the PDP, as done previously in the literature. After analyzing the drawbacks of this approach, we propose working with the LSF and clustering algorithms for scatterer identification. Working with the LSF we study a new domain Doppler Shift and we can extract different parameters related to this domain as the extension of the cluster.

Visual inspection on Power Delay Profile

After analyzing and understanding the previous work that had been carried out on vehicular communications, I began studying the PDP by visual inspection, in order to identify the relevant scattering objects.

By making use of the videos recorded during the measurements, the different multipath components observed in the PDP can be *visually* analyzed and related to physical objects which interact with the radio waves during the measurements.

However, working with visual inspection is not the best solution. There are scenarios where it is clear and easy to identify the different contributions and to know where they come from. But in other cases the task becomes too difficult to be done *visually*. It would be smarter to define a way where the identification works in an automatic manner.

Detection peak on LSF

In order to overcome the drawbacks of the previous method, I propose toe analyze the LSF. By doing so, we introduce in the analysis another domain, the Doppler shift, which gives accuracy in the scattering identification. As we commented before, each peak of this plot represents a different path.

First of all we have to distinguish only the more relevant paths from the received signal. Figure 17 (a) show another view of the LSF seen from the side for a given time instant. It is possible to observe that there are several peaks that are not important, they are not relevant if you compare with the highest peak. We used a very simple concept, the power threshold criterion [22]. A path can only exist when it has more power than a certain threshold. We chose the threshold as the highest detected peak minus 20 dB. We consider that it is enough and has been crosschecked using the visual inspection approach. Another threshold was required to remove the noise. All components below power noise plus 15 dB is set up a 0. In Fig. 17 (b) we present the different thresholds.

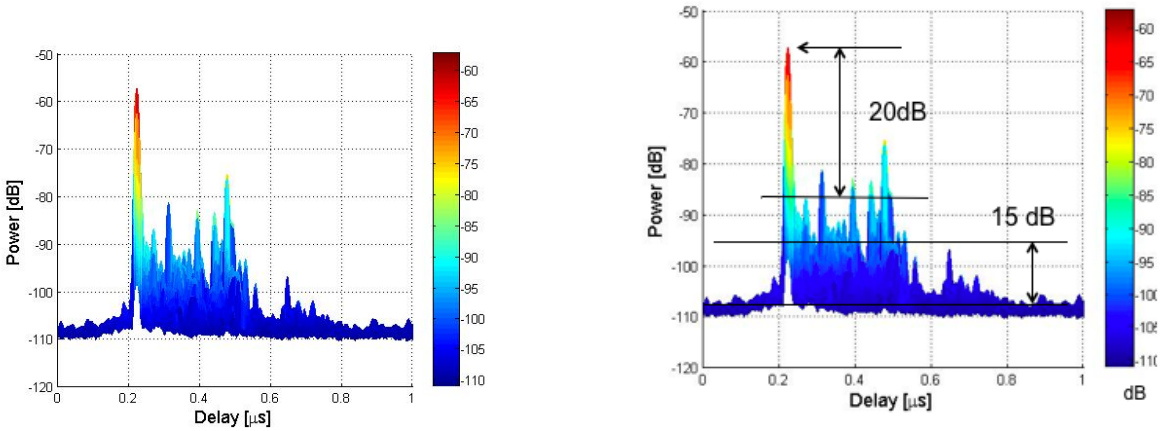

(a) LSF without applying power and noise thresholds

(b) LSF with power and noise thresholds applied

Figure 17: 2D view (Power-delay) of the LSF for one time instant.

In Fig.18 the different detected paths are shown as red crosses over the 2D view (delay-Doppler shift) of the LSF for a given time instant. In this experiment our algorithm can detect

five path.

In Fig. 18 (a) we observe that each one of the scatterers contributions is defined by several multipath components. For each scattering object we can group the multipath components in clusters, as shown in Fig. 18 (b). By using already existing algorithms, we can relate each one of the multipath components to one cluster. With that, we are going to be able to identify not oly the number of relevant scatterers (number or clusters) but also their extension in delay and Doppler shift domains.

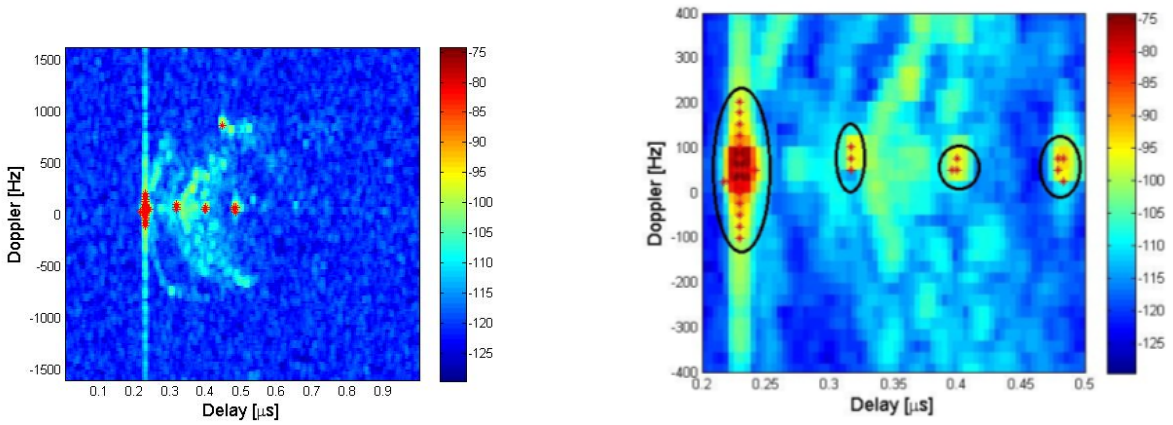

(a) Identification path on LSF

(b) Identification clusters

Figure 18: Peak detection on LSF

6.6.2 Cluster identification algorithms

We would like to develop a method for identifying the number of relevant paths, and for each path, its extension in the two domains, delay and Doppler shift.

To achieve our aim we analyze several clustering algorithms, which can be classified into two categories: partitioning algorithms, and hierarchical algorithms. We will describe them in the following.

Partitioning algorithms

They construct a partition of a database D of n objects into a set of k clusters. k is an input parameter for these algorithms. They start with an initial position of D and then uses an iterative control strategy to optimize an objective function. Depending on where the center of the cluster is placed, the partitioning algorithms can be further classified into:

[*k-means algorithms*:] Each cluster is represented by the gravity center of the cluster, or

[*k-medoid algorithms*:] Each cluster is represented by one of the objects of the cluster located near its center.

Hierarchical

is a method to build a hierarchy of clusters of D. Strategies for hierarchical clustering generally fall into two types:

[*Agglomerative*:] This is a "bottom up" approach: each observation starts in its own cluster, and pairs of clusters are merged as one moves up the hierarchy.

[*Divisive*:] This is a "top down" approach: all observations start in one cluster, and splits are performed recursively as one moves down the hierarchy.

The results of hierarchical clustering are usually presented in a dendrogram, a tree that iteratively splits D into smaller subsets until each subset consists of only one object. In such a hierarchy, each node of the tree represents a cluster of D.

We studied in depth three different clustering algorithms, all of them belonging to the partitioning algorithms family. Next, we describe them shortly and explain whether they are useful for our purpose.

KPowerMeans algorithm

To be able to identify clusters both more quickly and accurately, the concept of the K-means algorithm is well suited for this challenge. We use the Multipath Component Distance (MCD) [22], which allows to combine parameters that come in different units.

$$MCD_{ij} = \sqrt{MCD_{\tau,ij}^2 + MCD_{\upsilon,ij}^2 + MCD_{power,ij}^2} \tag{12}$$

where $MCD_{\tau,ij} = \zeta_\tau dist_{euclidian}$, $MCD_{\upsilon,ij} = \zeta_\upsilon dist_{euclidian}$ and $MCD_{power,ij} = \zeta_{power} dist_{euclidian}$.

The KPowerMeans algorithm, which introduces the novelty of regarding powers of the multipath components. This algorithm iteratively minimizes the total sum of power-weighted distances of each path to its associated cluster centroid. In the following the single steps of the algorithm are described in more detail.

- The centroid starting positions are chosen randomly from the data X.
- Every multipath component is associated with a cluster centroid such that the function of the total sum of differences,

$$D = \sum_{l=1}^{L} P_l MCD(x_l, \mu_{I_l(i)}), \tag{13}$$

  is minimized . We use the MCD as the basic distance function but also include the power of the paths. The index $I_l^{(i)}$ is the cluster number for the ith multipath in the ith iteration step.

$$I_l^{(i)} = argmin[P_l MCD(x_l, \mu_c^{(i-1)})]. \tag{14}$$

  By including power into the distance function, the points cluster with strong powers are composing the centroids. Being the denation for a cluster in KPowerMeans algorithm:

  For a given number of clusters, clusters are chosen such that they minimize the total distance from their centroids.

- The centroids move to the centers of gravity of the groups of multipath components allocated in the previous step. Note that moving centroids can result in a new group of multipath components that will be associated with the centroid in the next iteration step.
- If the centroids do not move any more the algorithm has converged to a stable solution. If this procedure take too much time, it stops after a defining maximum number of iterations already defined.

- The output of the algorithm is the index set $I^{(i)}$ and the associated cluster centroids $\mu_c(i)$, which were obtained by the last iteration.

In the end, we did not use this algorithm because of we could not find out a common weighted factor for all the scenarios.

Substractive clustering algorithm

The subtractive clustering method assumes that each data point is a potential cluster center and calculates a measure of the likelihood that each data point would define the cluster center, based on the density of surrounding data points[23] . The algorithm does the following:

- Selects the data point with the highest potential to be the first cluster center.
- Removes all data points in the vicinity of the first cluster center (as determined by radii), in order to determine the next data cluster and its center location.
- Iterates on this process until all of the data is within radii of a cluster center.

The subtractive clustering method is an extension of the mountain clustering method proposed by R. Yager.

We discard this algorithm because we could not find a common radii for all scenarios. We should note that for experiments with few clusters the algorithm works really well, but when we apply the algorithm in experiments with a large number of clusters the algorithm is not reliable.

Density-based spatial clustering of applications

The Density-based spatial clustering of applications (DBSCAN) algorithm [**?**] is designed to discover clusters of arbitrary shape and it requires only one input parameter and supports the user in determining and appropriate value for it. Moreover, DBSCAN is efficient for large spatial database.

The key idea is that for each point of a cluster the neighborhood of a given radius (Eps) has to contain at least a minimum number of points (MinPts), i.e. the density in the neighborhood has to exceed some threshold. The shape of a neighborhood is determined by the choice of a distance function for two points p and q, denoted by $dist(p, q)$.

To find a cluster, DBSCAN starts with an arbitrary point p and retrieces all points density-reachacle from p with respect to Eps and MinPts. If p is a core point, this procedure yields a cluster wrt. Eps and MinPts. If p is a border point, no points are density-reachable from p and DBSCAN visits the next points of the database.

DBSCAN discovers the clusters and the noise in a spatial database according to next definitions,

First description - cluster

Let D be a database of points. A *clusterC* with respect to Eps and MinPts is a non-empty subset of D satisfying the following conditions:

- $\forall$ p,q: if p $\in$ and q is density-reachable from p with respect to Eps and MinPts, then q $\in$ C. (Maximality)

- $\forall$ p,q: if p $\in$ and q is density-connected to q with respect to EPS and MinPts. (Connectivity)

Second description - noise

Let $C_1, ..., C_k$ be the clusters of the database D wrt. parameters Eps_i and $MinPts_i$, i = 1,...,k. Then we define the *noise* as the set of points in teh database D ot belonging to any cluster C_i.

We chose the algorithm parameters as MinPts is 1 and Eps 7, with these values we observed that the algorithm worked as we expected. MCD is the used distance was used as we defined in Eq. 12, but in this case the power term was not necessary. Since we observed that the clusters are larger in the Doppler domain we give more importance to it by setting the weighting factors to ζ_v using $\zeta_v = 6$ and $\zeta_\tau = 5$. We observed good results with this algorithm for the training and the validation data sets, therefore we decided to carry out our time-varying clustering parameter analysis with the DBSCAN algorithm.

6.6.3 Time-varying cluster parameters

After we chose the appropriate cluster algorithm we are going to extract the following parameters: number of clusters, and extension of the cluster in delay and Doppler shift domains.

Number of clusters

It will be interesting to know the number of clusters identified in each experiment, which indicates the number of relevant scattering objects.

Cluster extension in delay and Doppler

We are also interested in finding the extension of each cluster in delay and Doppler domains. Since the scenario is highly time-varying, the cluster parameters are going to be time-varying as well. We make here a very simple classification of the clusters between the first observed cluster (the one with minimum delay) and the rest. This is necessary due to the different characteristics observed between them, as we will see in the next chapter.

For each experiment, we will calculate the temporal expected value over the whole measurement run. Afterwards we will present the mean value over all experiments per scenario. Based on these results, conclusions will be drawn.

7 Results

7.1 Methodology

Our work starts with the DRIVEWAY campaign , where we have 76 experiments. The experiments can be grouped into 5 different scenarios as described in section 5.3. In order to develop a method to be applied to data, we need to distribute the data into three groups:

- Training data set: It is used for designing the algorithm (i.e. finding the right values for the input parameters.)
- Validation data set: It is used for checking the correctness of the chosen parameters.
- Application data set: It is composed by the rest of the data to be analyzed.

Figure 19 shows the final distribution.

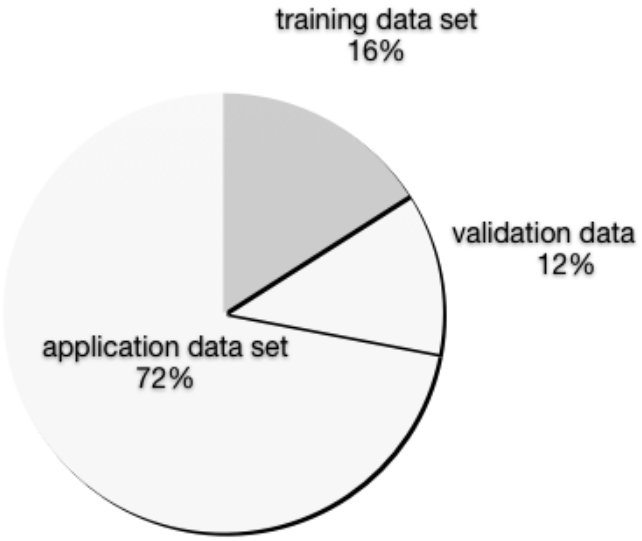

Figure 19: Distribution of data set

We used 16 per cent of measures were for training data set. This number belong to General LOS obstruction scenario. In this situation the cars are driving on a highway and the different paths are very easy to identify, so we used this scenario for the visual inspection. Finally, we confirmed that the results obtained by our algorithms were correct because we had already the visual inspection results.

The 12 per cent of the data is the merging lanes scenario. And we used this situation to validate the data set. We chose it because also the cars are driving in a highway and the situation was similar to the scenario previously studied. Here we also checked the results obtained by the algorithms using the visual inspection.

Finally, we apply the algorithm to the rest of the data set, being 72 per cent of the total data.

7.2 Results

This section presents the results of the parameters described in sections 6.5 and 6.6 for each scenario. In this report makes a thorough study of an experiment for each scenario but at the end of each section are defined scenario conclusions.

7.2.1 PDP and DSD

Next, the PDP and DSD for each scenario will be discussed. We are going to analyze different situations and understand the multipath propagation.

Scenario 1.1 - Road crossing: Open area rural

In this situation we want to study the behavior of the channel when the cars are in a road crossing. In this case, it is in a open area (rural). Both cars are driving from different streets ending towards the same crossing, where there is a traffic light. Finally, the TX and RX are stopping at traffic light.

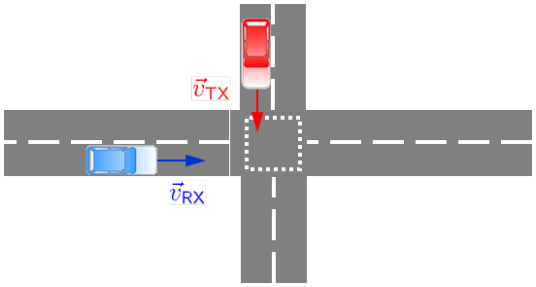

Figure 20: Situation: Road crossing- rural area

PDP and DSD

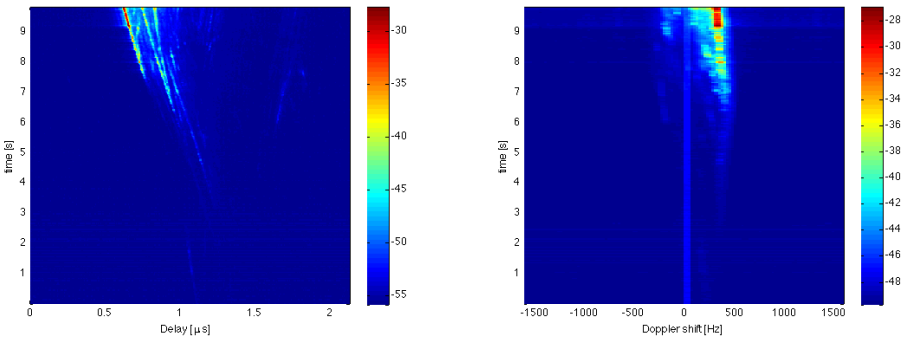

(a) PDP (b) DSD

Figure 21: PDP and DSD: Road crossing- urban area

In the 6 first seconds of Fig. 21 (a), there is not communication between the cars, because they are far away from each other. And there are buildings that interfere in the communication. When they have a visual contact, the communication starts. Every instant that the cars are approaching to the crossing the delay is decreasing. We recognize different contributions produced from the reflections with different objects (a van, a bus, and buildings). The other plot shows the DSD, as long as the cars are approaching the DSD is positive around 500 Hz.

Scenario 1.2 - Road crossing: Suburban

Now we want to study the road crossing situation but when there is obstructed LOS in a suburban area. In one corner of the crossing there are buildings, otherwise the environment is a open surroundings. The cars are approaching to the crossing from different streets.

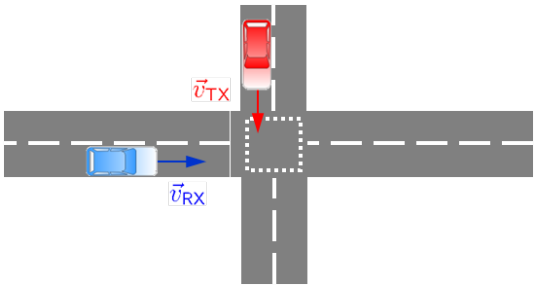

Figure 22: Situation: Road crossing- Suburban

PDP and DSD

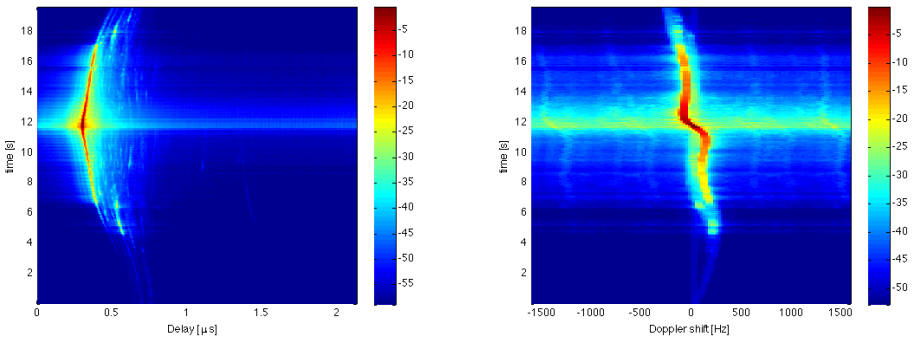

(a) PDP (b) DSD

Figure 23: PDP and DSD: Road crossing- suburban

Figure 23 (a) presents the PDP of this situation. We start to get communication at 4 s, before the cars are too far from each other and the buildings intercept the communication. After that and during 3 s, the cars are approaching to the crossing and the RX stats to receive information. When they get the signal with more power is when they are passing. At 13 s, the cars are leaving the crossing behind them and consequently the delay increases again. In this scenario is rich in diffuse components caused by buildings and trees.

The DSD is shown in Fig. 23 (b), the Doppler component is positive around 250 Hz while the cars are approaching to the crossing. It starts to get negative when the cars are leaving from the crossing.

Scenari 1.3 - Road crossing: Urban - Single lane

In this section, we present another road crossing subscenario. TX and RX are in a urban environment with obstructed LOS and surrounding buildings. They are driving from different single lane streets to the same crossing. TX stops at the crossing letting the RX drives.

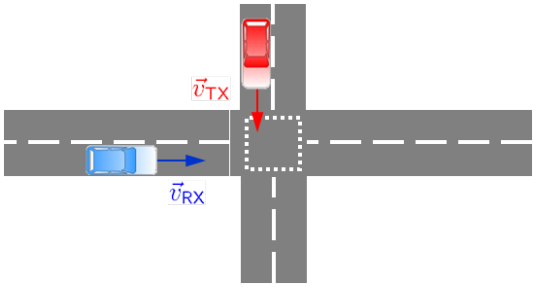

Figure 24: Situation: Road crossing- urban: single lane

PDP and DSD

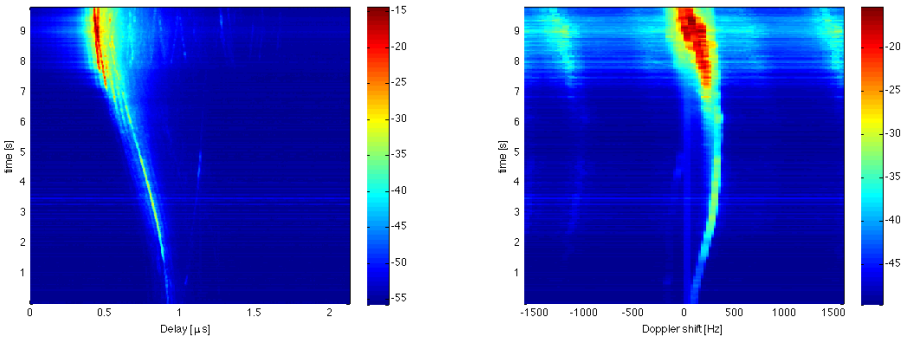

(a) PDP (b) DSD

Figure 25: PDP and DSD: Road crossing- urban: single lane

Figure 25 (a) presents the PDP in a typical road crossing in a urban environment. The first 7 s TX and RX are approaching to the crossing from different ways. And the delay starts with 1 μ s until 0.5 μs. After 7 s the cars have LOS because they are in the crossing and again the scenario is rich in diffuse components.

In Fig. 25 (b) when the cars approaching the Doppler shift is positive. When they are closer to each other the Doppler shift is decreasing until 0 Hz.

Scenario 1.4 - Road crossing: Urban - Multiple lanes

This is the last scenario where we want to study the behavior of the channel in a road crossing. In this case, the cars are driving in an urban environment with obstructed LOS and surrounding buildings. TX and RX are driving from different multiple lanes street to the same crossing. RX is stopping at the crossing and TX is crossing following a bus.

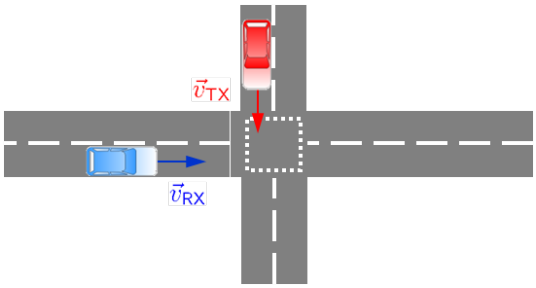

Figure 26: Situation: Road crossing- urban: multiple lanes

PDP and DSD

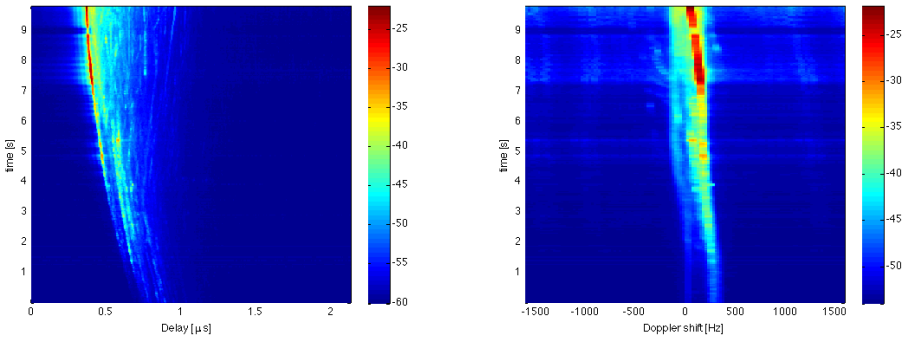

(a) PDP (b) DSD

Figure 27: PDP and DSD: Road crossing- urban: multiple lanes

We can see in Fig. 27 (a), that the communication between the cars starts at 1 s when they do not have visual contact and they are approaching to the crossing. The power is weak and there are several diffuse components. At 7 s when suddenly the power increases, it starts the visual contact between the TX and RX. Urban scenarios are rich in diffuse components.

The Doppler shift (Figure 27 (b))starts around 250 Hz and it is decreasing until 0 Hz when the RX is stopping and the TX is crossing.

Scenario 2 - General LOS obstruction

In this experiment TX and RX are driving in the same direction on the highway with similar velocities v_{TX} and v_{RX}, respectively, and one truck is driving between them blocking the LOS. Also several trucks are driving in the same direction as the cars and in the opposite direction, they are causing the most of the relevant multipath components. Around the highway there are

not too much obstacles that could not influence the propagation. For that reason this scenario is good for detecting the different scatterers. We used this scenario as a training.

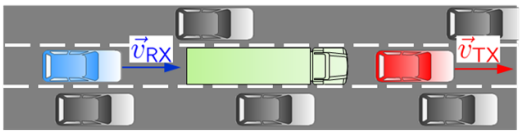

Figure 28: Situation: General LOS obstructed

PDP and DSD

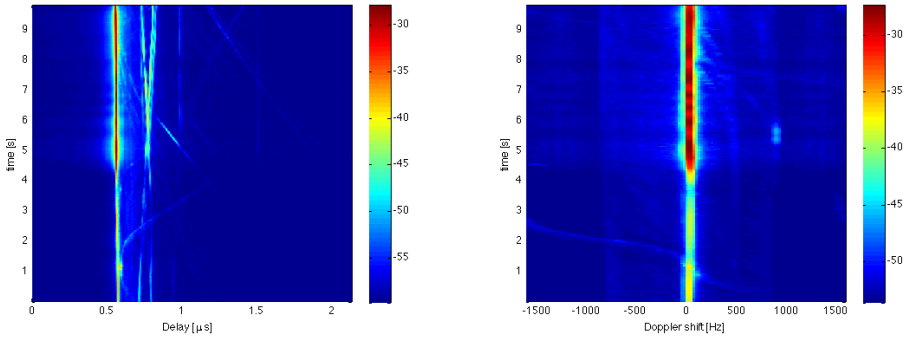

(a) PDP (b) DSD

Figure 29: PDP and DSD: General LOS obstructed

Figures 29 (a) and (b) show the PDP and the DSD for a typical situation of LOS obstructed. The TX drives in front of a truck at about 80 km/h and the RX is behind this truck and drives at about 90km/h. During the measurement run, which lasts 10 seconds, the truck in between the two cars moves away thus not obstructing the LOS anymore.

It is possible to identify 5 relevant multipath contributions. The first path that we observe, with the smallest delay, has the highest power. We clearly differentiate two intervals with different signal strength. The first interval starts at 0 s and lasts until 4.2 s and corresponds to the time when the truck is between the TX and RX , the LOS is blocked and the signal is diffracted on the roof surface of the truck. In the second interval, between 4.2 s and 10 s, the signal strength increases, because of the truck driving between the TX and RX has changed the lane, leaving LOS between the cars. This phenomena becomes even more evident in the DSD, where the Doppler shift remains constant at 0 Hz since the relative speed between TX and RX is always around 0.

The second path corresponds to another truck that is driving in the opposite direction. We identify three important intervals. During the first interval, the truck is approaching the TX from 0 s until 0.8 s and the delay of the path decreases. The Doppler shift is positive with decreasing value as the truck gets closer. Then the truck is between the cars during almost 1 s. In the PDP we observe a component constant very close to the LOS. In the DSD, the Doppler shift stays around 0 Hz. Finally, around 4 s, the truck moves further away, so the delay increases again until it fades out with the received power of the path, the Doppler shift becomes negative and increases as the truck leaves. These three intervals can be easily identified in Fig. 29.

The TX has another truck in front driving at a constant speed, the signal reflection on it causes the third path. One more time, we observe that the signal is stronger at 4.2 s, owing to the fact that the truck driving between TX and RX changes the lane, and unobstructs the LOS. Since the relative speed between TX-RX and the truck is constant, the Doppler shift component of this path is at 0 Hz and can not be differentiated in the DSD plot.

We suppose that the fourth path is originated by an object left behind the RX, probably another truck driving behind. The Doppler component is not observable due to the same reason as in the third path.

Finally, the last path is caused by another truck approaching to the TX-RX in the opposite direction, similar to the second path. The signal strength of this path is high between 5 and 6 seconds, the Doppler shift of this component becomes clear only during that time interval, with a positive value of 1000 Hz. When comparing the second and the fifth paths, we can say that the truck causing the second path drives much faster. This can be observed in the curvature of the delay component in the PDP and the value of the initial Doppler shift.

Scenario 3 - Merging lanes

In this experiment, the RX is driving in the highway and TX wants to access in. For entering in the highway first the car should drive under a bridge and then take a road with several trees between it and the highway. There are not trucks or other objects which cause multipath components.

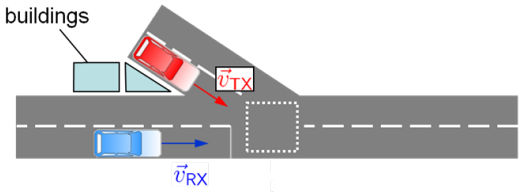

Figure 30: Situation: Merging lanes

PDP and DSD

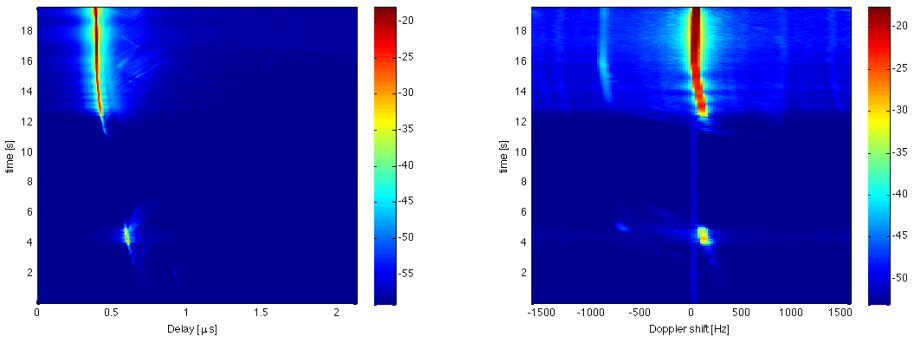

(a) PDP (b) DSD

Figure 31: PDP and DSD: Merging lanes

When the communication starts, they have vision during one second at 4 s, is when one car is over the bridge and the other car has just passed the bridge. After that they do not have visual contact because there are plenty of trees between them, and they lose the communication during 6 s. Finally, they get the communication when the TX access in the highway with a strong power. After 14 s it is possible to identify a scatter from a truck driving from the opposite direction and it is approaching to the TX.

From Fig. 31 we realized that when the cars are one in front of the other Doppler shift is around 0 Hz as 16 s until 20 s. At 4 s the TX is driving for the road that give access in the highway, so the cars are approaching and the Doppler shift is around 100 Hz.

Scenario 4.1 - Traffic congestion: Slow traffic

In this scenario we want to study how the channel behaves when cars are in a congested traffic situation. More specifically, in slow traffic. The TX and RX are on the same lane and between them there are four cars and a high van. When the communication starts, the TX is located under a bridge and in front of it has a truck.

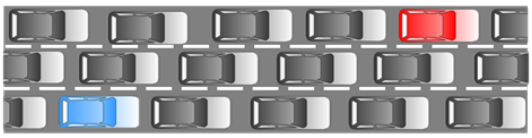

Figure 32: Situation: Traffic congestion- Slow traffic

PDP and DSD

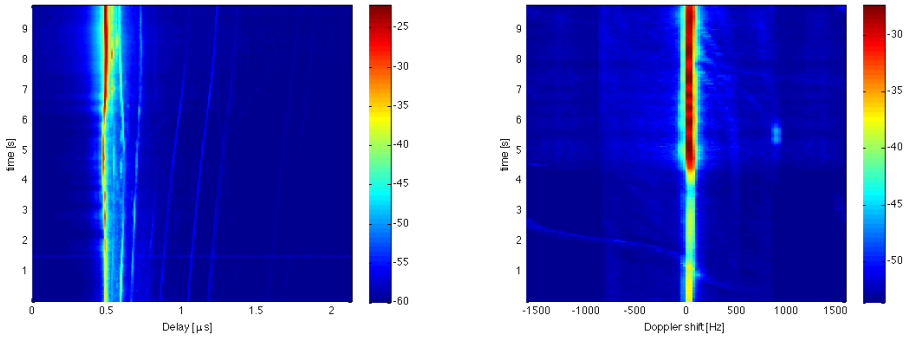

(a) PDP (b) DSD

Figure 33: PDP and DSD: Traffic congestion- Slow traffic

Figure 33 (a) shows the PDP of this experiment, we identify the LOS at 0.5 μs and we distinguish two intervals. The communication starts when the TX is under the bridge and it remains there during 6 s, in this interval the power is not really good. In the second interval the TX is not under the bridge anymore and the power increases.

We identify some MPCs, one of them (at around 0.7 μs) comes from the truck which is in front of the TX. The other MPC is not possible to know where it comes from, but probably

from some traffic sign that we are leaving behind or some truck in front of the TX and RX in the other lane and it is moving faster than us.

Figure 33 (b) presents the DSD, where we only see the LOS and also we can distinguish the two intervals. The Doppler shift is 0 during the first 7 s because the cars are moving with similar velocity. At 7 s the RX stops and the TX keeps moving and then the DSD start to be a positive value.

Scenario 4.2 - Traffic congestion: Approaching traffic jam

In this scenario the cars are driving on a highway and we want to study the traffic congestion. The TX is stuck on the traffic jam on the right lane and it is moving really slow, and RX approaches from behind on the left lane at very slow speed. There are around 15 cars in between, but in the end the RX arrives to the same point where the TX is.

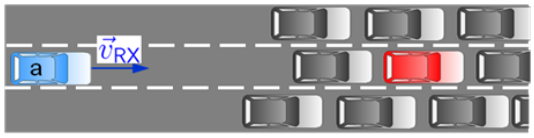

Figure 34: Situation: Traffic congestion- Approaching traffic jam

PDP and DSD

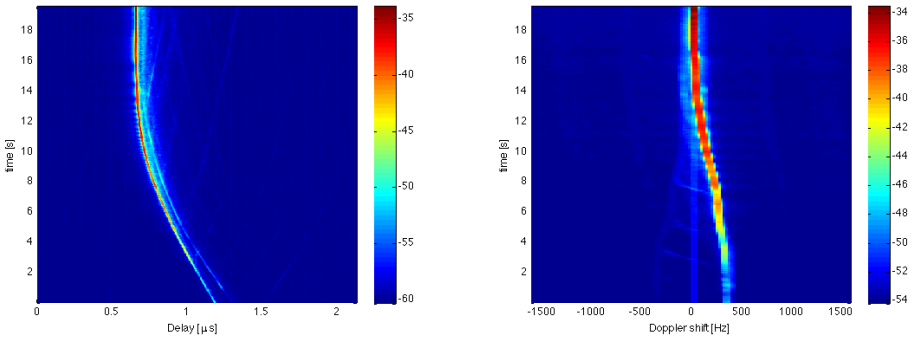

(a) PDP (b) DSD

Figure 35: PDP and DSD: Traffic congestion- Approaching traffic jam

If we observe Fig. 35 (a), three different intervals are distinguished in the PDP. The first interval is during the first 10 s, where the RX is approaching to the traffic congestion with higher speed than the TX. And we can see how the delay is decreasing. The second interval is the next five seconds (10-15 s), where the RX is still approaching to the TX but now it is inside the traffic congestion driving slower than before. And finally, the rest of the time the RX is next to the TX trying to overtake it. Also, we realized that power increases with the distance and when the RX is in the traffic jam appear diffuse components. To conclude, there is a MPC with the same behaivour as the LOS but with more delay, probably one truck or van is behind the TX.

Talking about the DSD, we also observe the three intervals. When the RX is approaching to the RX the Doppler shift is positive around 400 Hz, and it starts to decrease to 0 Hz when the cars are next to each other.

Scenario 5 - In-tunnel

In this scenario we want to characterize the channel when the cars are into a tunnel. There are not cars or trucks in this situation. TX is diving 120 m in front of the RX.

PDP and DSD

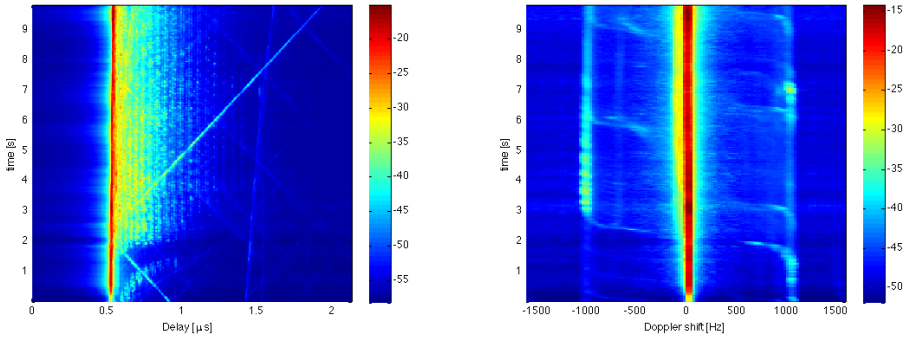

(a) PDP (b) DSD

Figure 36: PDP and DSD: In-tunnel

We can see in Fig. 36 (a) the strong LOS because between the cars there is not any obstacle that interfere in the communication. It is odd that appear periodic MPC parallel to LOS caused for the reflection of the tunnel wall, each one with different delay and the power is decreasing with the delay. The first second the cars are not into the tunnel and we do not have the reflections which we already comment. There is an object approaching during 2 s and at 3 s the cars are leaving it. This strong path is caused by a metal wall on the roof in the entrance of the tunnel.

Figure 36 (b), LOS has 0 Hz. It is possible to identify the strong MPC that we were commenting, before the cars have not entered to the tunnel (first 2 s) Doppler shift is 1000 Hz, but when they are inside the tunnel and the RX is leaving the object behind him the Doppler shift is negative with 1000 Hz.

Scenario 6 - Bridge

Finally, in the last situation we want to characterize the channel when the cars are over a bridge. TX is driving in front of the RX with similar speed. In Fig. 38 shows the bridge where the data was took.

PDP and DSD

Figure 37: Situation: Bridge

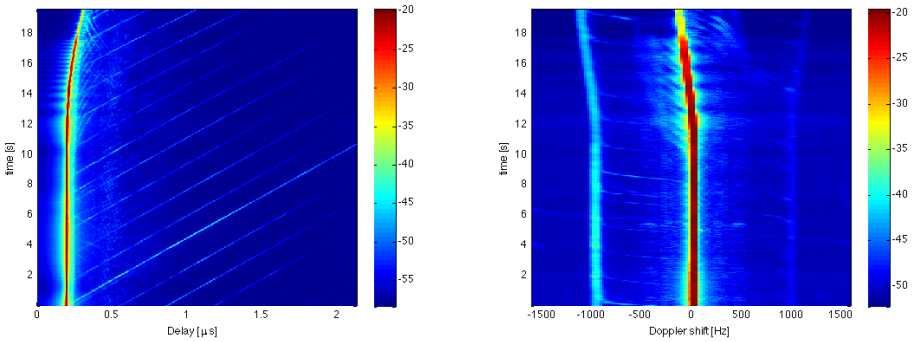

(a) PDP (b) DSD

Figure 38: PDP and DSD: Bridge

Figure 38 (a) presents the PDP in this situation. LOS has 0.25 μs and a strong power. The cars are driving with the same speed during 12 s, but after that the TX wins speed and the LOS delay increases. Curiously, there are a periodic MPC in all the range of data. They are caused by the streetlights which are in the center of the bridge. In 38 (b), LOS has Doppler shift 0 Hz the first 12 s and then it starts to get negative value because the TX gets velocity. The MPC have Doppler shift 1000 and -1000 Hz, when the cars are approaching to the streetlight and when they are leaving it, respectively. Being the MPC with Doppler shift -1000 Hz the ones with stronger power.

7.2.2 Time-varying rms delay spread

In this section we study the behavior of rms delay spread and how it is related to the PDP. We already advance that at the end of this section we note that the rms delay spread becomes important at time intervals where there are more MPCs. In the annex 10.1 we find the average and maximum values for each experiment.

Scenario 1: Road crossing

Figure 39 (a) shows the rms delay spread which increases at 7 s during one second. Being this interval the one with more MPCs and getting the maximum value (93.02 ns) in this range. Next, the rms delay spread decreases until 50 ns and remains oscillating around this value. This happens in the moment when the LOS in the PDP has the maximum power.

To analyze the rms delay spread 39 (d) it is interesting to compare it with the PDP 39 (c). The rms delay spread is oscillating around 15 ns while the LOS contribution has the highest power. At 6 and 18 s, rms delay spread gets the maximum values when some diffuse components increase their power.

The rms delay spread (Fig. 39 (f)) starts around 10 ns and it is growing slowly until 60 ns. There are three peaks in the picture and coincide with a MPC that gets importance at 0.5 s and at 4 until 5 s.

The rms delay spread in (Figure 39 (h)) is more or less stable. It becomes bigger with the diffuse components. On the other hand, it decreases when the power gets importance. At 9 s, there is a peak because in this time instant the power suddenly becomes worse.

Scenario 2: General LOS obstructed

As shown in 40 (b), the rms delay spread oscillates around 46 ns but it decreases when the multipath components lose power, at around 2 and 4 s.

Scenario 3: Merging lane

The rms delay spread increases suddenly when the first communication getting almost the highest rms delay spread. After that, the signal disappears during 6 s because of the trees between the cars. At 11 s we receive signal and the rms delay spread keeps oscillating around the 20 ns getting the highest peak around 16 s when there is a multipath component coming from a truck.

Scenario 4: Traffic congestion

In Fig. 42 (b) the rms delay spread is presented. We can easy distinguish the two intervals. The first 7 s, it is where the rms delay spread has the maximum value 51.49 ns, but it is oscillating around 37 ns. Each peak that we see is produced when the MPC get more importance, when the power is higher. In the second interval, when the LOS has the maximum power the rms delay spread decreases around 23 ns.

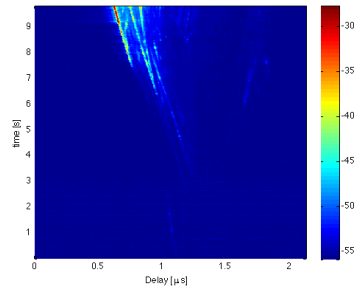

(a) PDP for scenario 1.1

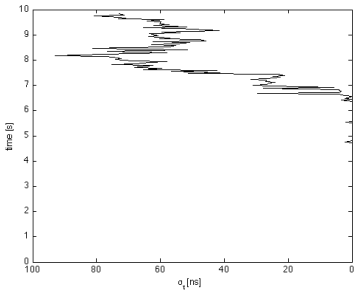

(b) rms delay spread for scenario 1.1

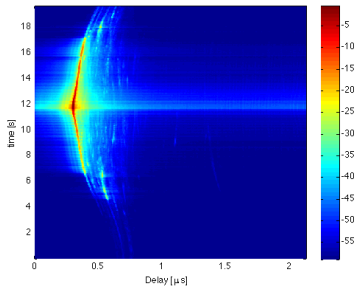

(c) PDP for scenario 1.2

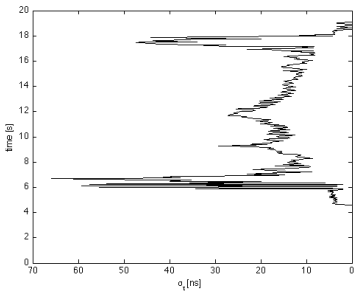

(d) rms delay spread for scenario 1.2

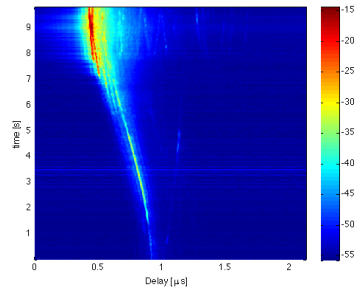

(e) PDP for scenario 1.3

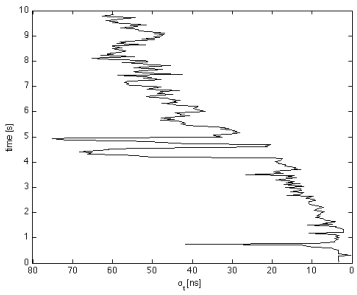

(f) rms delay spread for scenario 1.4

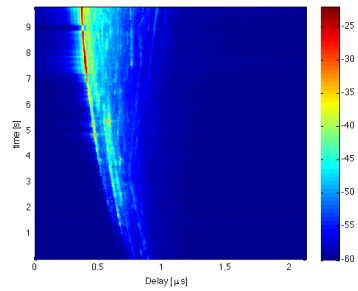

(g) PDP for scenario 1.4

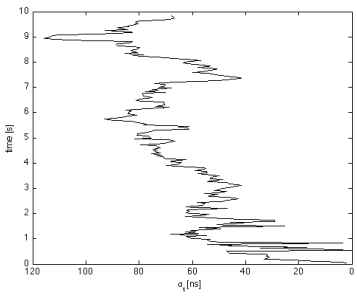

(h) rms delay spread for scenario 1.4

Figure 39: PDP and rms delay spread for scenario 1

The rms delay spread in Fig. 42 (d) is oscillating around 14 ns, and the peaks of the first interval are related to increased the MPC power.

Scenario 5: In-tunnel

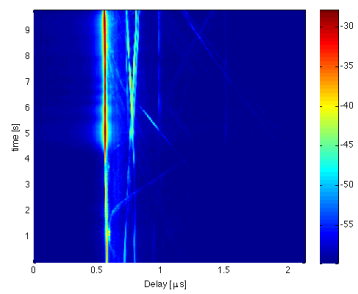

(a) PDP for scenario 2.1

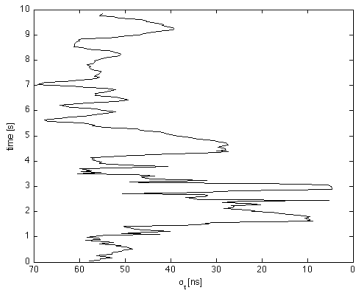

(b) rms delay spread for scenario 2.1

Figure 40: PDP and rms delay spread for scenario 2

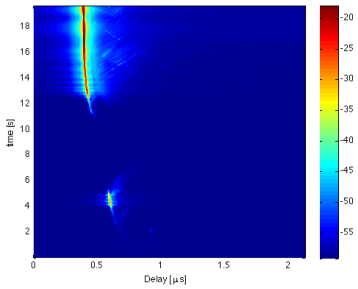

(a) PDP for scenario 3.1

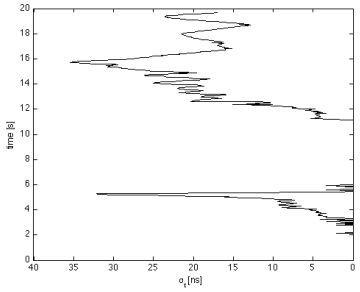

(b) rms delay spread for scenario 3.1

Figure 41: PDP and rms delay spread for scenario 3

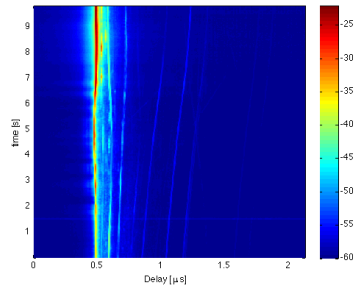

(a) PDP for scenario 4.1

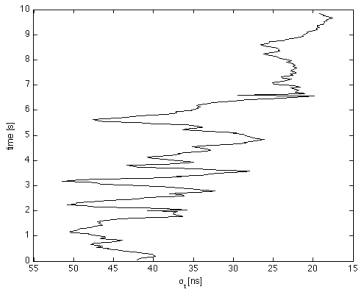

(b) rms delay spread for scenario 4.1

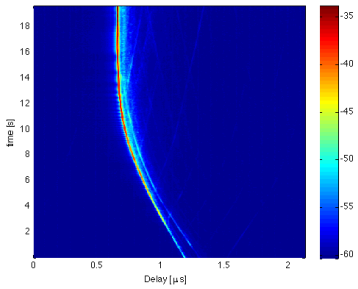

(c) PDP for scenario 4.2

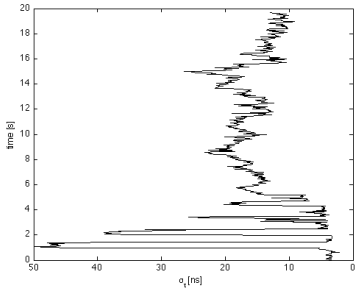

(d) rms delay spread for scenario 4.2

Figure 42: PDP and rms delay spread for scenario 4

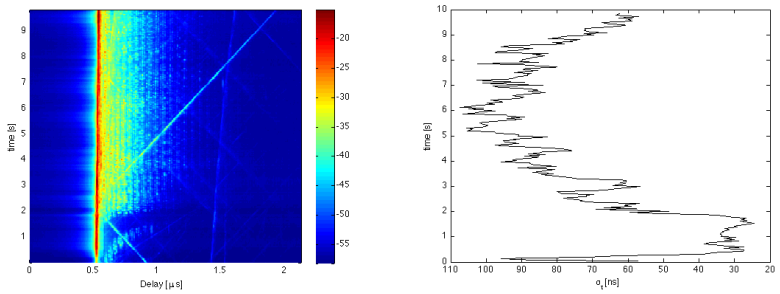

(a) PDP for scenario 5.1 (b) rms delay spread for scenario 5.1

Figure 43: PDP and rms delay spread for scenario 5

In this experiment the rms delay spread 43 (a) is higher than in other scenarios because it is the scenario with richest diffuse components, being the maximum value 107 ns. When the communication starts, it gets around 95 ns, probably because of the strong LOS and the strong MPCs. Suddenly, it decreases to 30 ns, and at 2 s when the cars are inside the tunnel the rms delay spread starts to increase until it gets the maximum value because of the influence of the diffuse components.

Scenario 6: Bridge

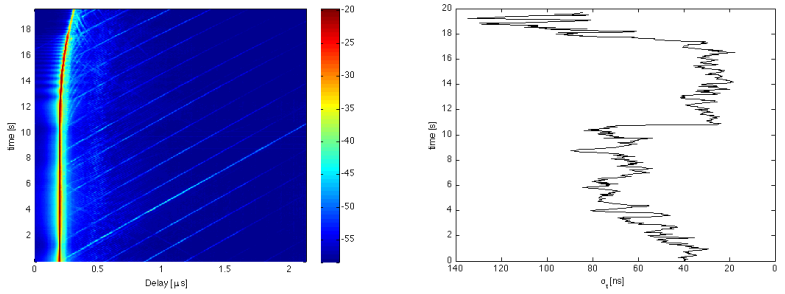

(a) PDP for scenario 6.1 (b) rms delay spread for scenario 6.1

Figure 44: PDP and rms delay spread for scenario 6

We observe three different intervals when we study the rms delay spread (Figure 44 (b)). During the first 11 s, the rms delay spread oscillates around 60 ns. Next, it decreases to 20 ns during 6 s because the strongest MPC disappears and the power of the LOS is high. When the power of the LOS starts to be weak the rms delay spread gets high again obtaining the maximum value.

7.2.3 Rms delay spread in various scenarios

Table 2 shows the average of rms delay spread in each scenario.

After having had a loot at the table, we can observe that the mean of rms delay spread is higher in urban areas than in suburban or rural areas. This conclusion is what we were expecting, because in urban areas there are more objects causing the MPCs.

Table 2: Rms delay spread in various scenarios

Scenarios	$\bar{\sigma_\tau}[ns]$
Road Crossing: Area rural	25.63
Road Crossing: suburban	19.17
Road Crossing: urban - single lane	38.43
Road Crossing: urban - multiple lanes	53.44
General LOS obstruction	39.52
Merging lanes	15.98
Traffic congestion: Slow traffic	22.79
Traffic congestion: Approaching traffic jam	14.29
In-tunnel	64.55
Bridge	86.510

If you take a look in the four subscenarios of Road crossing, the road crossing in urban area with multiple lanes presents the highest rms delay spread in road crossing with 53.44 ns, and the minimum is in a suburban area is 19.17 ns.

If we compare the two next scenarios, both are in a highway, so we expect that the rms delay spread will be around the same value of suburban road crossing scenario. But, in case of general LOS obstruction the value is quite high, 39.52 ns, the reason for that is because the cars were driving beside several trucks and they produce MPC.

In traffic congestion scenarios the rms delay spread is smaller when cars are approaching to the traffic congestion, and finally, we can find the maximum value of rms delay spread 86.51 ns, in bridge scenario. Because it is the scenario with richest MPCs, most of them caused by the streetlights. Also the value from the in-tunnel situation is quite high because the walls of the tunnel are good reflectors.

7.2.4 Time-varying rms Doppler spread

In this section we study the behavior of rms Doppler spread and how it is related to the DSD. In this case, the rms Doppler spread becomes higher when there are diffuse components and when the signal power is strong. As for the rms delay spread, in the annex 10.1 we find the average and maximum values for each experiment.

Scenario 1: Road crossing

Conversely to rms delay spread, rms Doppler spread gets importance with the power of the signal. In Fig. 45 (b) the maximum value is at 9 s with almost 200 Hz when the power gets better. Before it remains around the 60 Hz.

Next scenario, (Fig. 45 (d)) increases when the power of the first path detected is higher, being the maximum value 285 Hz. This time is when the cars are in the crossing and they are passing each other. Otherwise, the rms Doppler spread is stable around 50 Hz.

We can see the same behaivour in urban areas. In Fig.45 (f), the rms Doppler spread remains stable around 20 Hz during 7 s. After that, suddenly, it increases getting to around 400 Hz. At that time is when we the cars have LOS and the maximum power and also when the diffuse

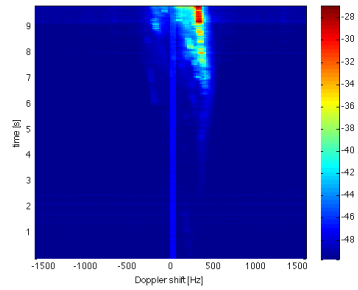

(a) DSD for scenario 1.1

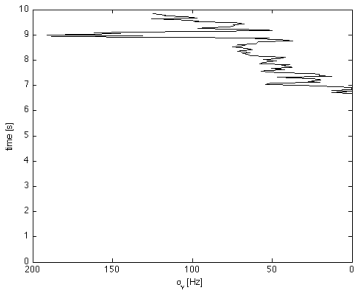

(b) rms Doppler spread for scenario 1.1

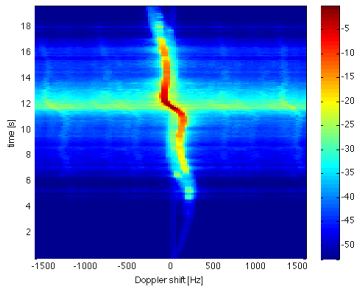

(c) DSD for scenario 1.2

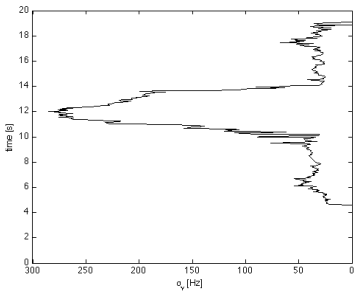

(d) rms Doppler spread for scenario 1.2

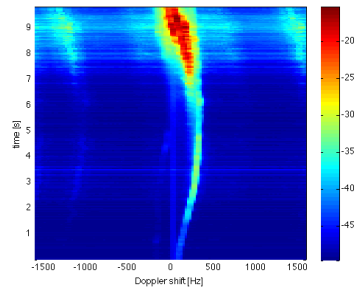

(e) DSD for scenario 1.3

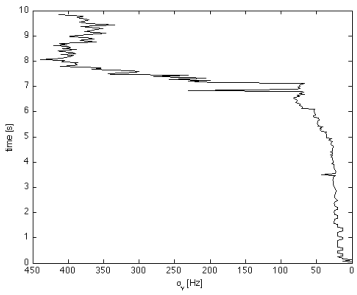

(f) rms Doppler spread for scenario 1.4

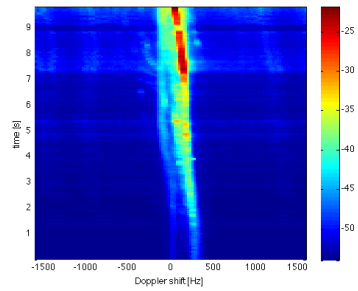

(g) DSD for scenario 1.4

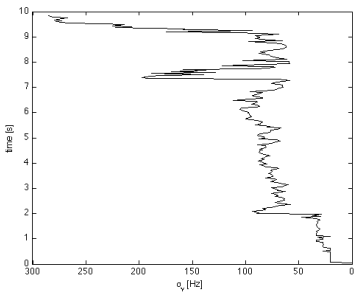

(h) rms Doppler spread for scenario 1.4

Figure 45: DSD and rms Doppler spread for scenario 1

components appear. Also in Fig. 45 (h) the rms Doppler spread grows when the power is stronger. And during the first 7 s it keeps stable around 75 Hz when the cars are far away from each other.

Scenario 2: General LOS obstruction

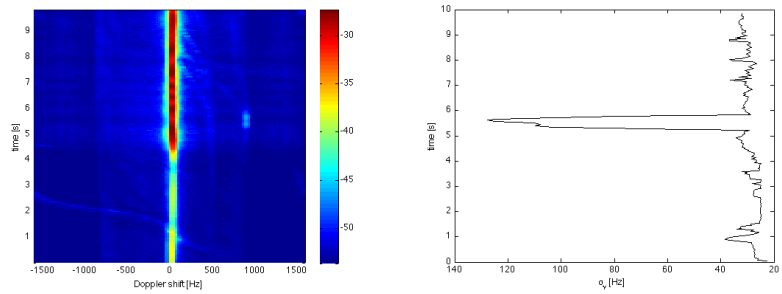

(a) DSD for scenario 2.1 (b) rms Doppler spread for scenario 2.1

Figure 46: DSD and rms Doppler spread for scenario 2

In plot 46 (b), we present the rms Doppler spread in a highway scenario. Where it remains stable around 33 Hz over the time. But at 5 s it increases suddenly when a new path appears with strong power.

Scenario 3: Merging lanes

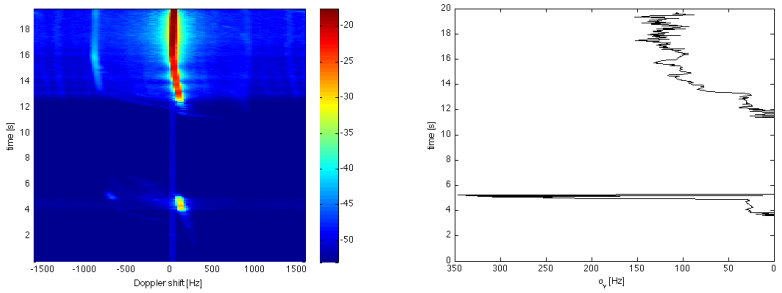

(a) DSD for scenario 3.1 (b) rms Doppler spread for scenario 3.1

Figure 47: DSD and rms Doppler spread for scenario 3

When there is the first communication, the rms Doppler spread increases strongly at 4 s getting the highest value 346.64 Hz. But in the second interval it remains stable around 125 Hz.

Scenario 4: Traffic congestion

Contrary to rms delay spread, rms Doppler spread give more importance to the power. The maximum now is in the second interval when the LOS increases. The rms Doppler spread oscillates over the time around 36 Hz. And the peaks that we can see are related with when the signal is stronger.

The rms Doppler spread also is oscillating around 27 Hz at 4 until 20 s, it is the time when LOS has a high power.

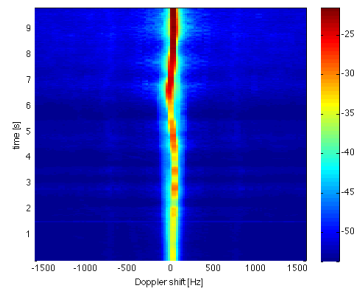

(a) DSD for scenario 4.1

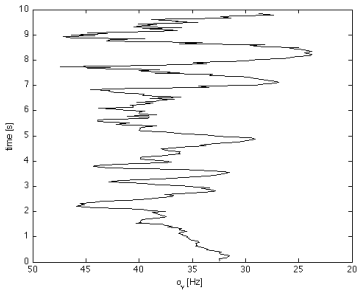

(b) rms Doppler spread for scenario 4.1

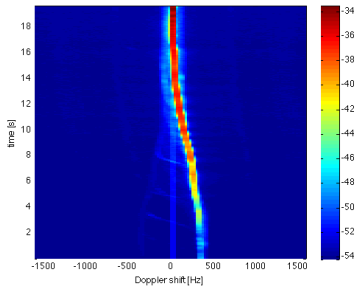

(c) DSD for scenario 4.2

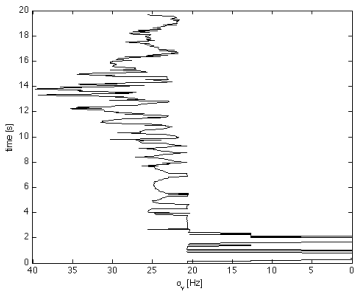

(d) rms Doppler spread for scenario 4.2

Figure 48: DSD and rms Doppler spread for scenario 4

Scenario 5: In-tunnel

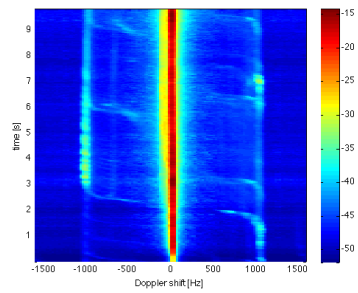

(a) DSD for scenario 5.1

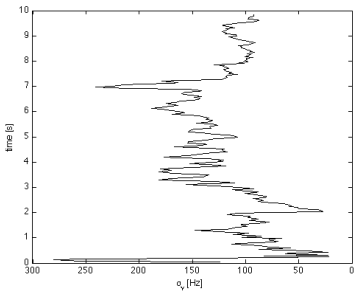

(b) rms Doppler spread for scenario 5.1

Figure 49: DSD and rms Doppler spread for scenario 5

The rms Doppler spread in tunnel remains oscillating over the time around 120 Hz. The maximum is in the first instant when the LOS has not a strong power.

Scenario 6: Bridge

In Fig. 50 (b), we show the rms Doppler spread, being stable during 17 s around 90 Hz. The last three seconds, suddenly it increases, getting the maximum value. The change is because some diffuse components appear and also the power of the LOS decreases.

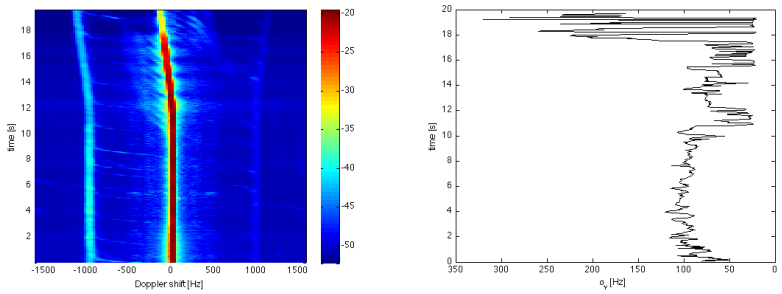

(a) DSD for scenario 6.1 (b) rms Doppler spread for scenario 6.1

Figure 50: DSD and rms Doppler spread for scenario 6

7.2.5 Rms Doppler spread in various scenarios

Table 3 shows the average of rms Doppler spread in each scenario.

Table 3: Rms Doppler in various scenarios

Scenarios	$\bar{\sigma_v}[Hz]$
Road Crossing: Area rural	65.08
Road Crossing: suburban	83.51
Road Crossing: urban - single lane	145.57
Road Crossing: urban - multiple lanes	74.33
General LOS obstruction	51.86
Merging lanes	76.38
Traffic congestion: Slow traffic	57.53
Traffic congestion: Approaching traffic jam	42.02
In-tunnel	111.12
Bridge	137.31

The first scenario, road crossing, we can notice as in rms delay spread that rms Doppler spread is highest in urban areas than in suburban, but we can not see a big difference. In the subscenario urban-single lane the rms Doppler spread is the maximum if we compare it to all other scenarios, the reason is that the diffuse components increase probably because the buildings are closer than in others scenarios.

In the highway scenarios, the value of the general LOS obstruction scenario do not surprise us, but, the value of the merging lanes it is higher than what we were expecting. It is probably because when there is signal the power is higher than in the other scenario because do not have any object between or around the cars.

In the rest of the scenarios, in-tunnel and bridge, the values are in the expected range, being the highest values after the road crossing - urban lanes.

7.2.6 Identifiability of wireless channels in all the scenarios

In this section we want to find out if all the scenarios are measurable. Table 4 shows that all our scenarios fulfilled Eq.11 from **??**, because the order of this product is around ms, so we are

in front of underspread channel and it can be measured.

Table 4: Identifiability of the different scenarios

Scenarios	$2\tau_{max}\upsilon_{max}[s \cdot Hz] \cdot 10^{-4}$
Road crossing: Area rural	0.59
Road crossing: Suburban	1.04
Road crossing: Urban - single lane	1.82
Road crossing: Urban - multiple lanes	1.19
General LOS obstruction	5.60
Merging lanes	0.97
Traffic congestion: Slow traffic	0.41
Traffic congestion: Approaching	0.93
In-tunnel	0.14
Bridge	0.24

7.2.7 Stationarity time in various scenarios

In this section we present the results of another channel parameter, the stationarity time. It is useful if we compare the different scenarios and try to find some conclusions. Furthermore, we can find in the annex **??** the average and some more figures. If we take a look at table 5, we see that there are two different values for the stationarity:

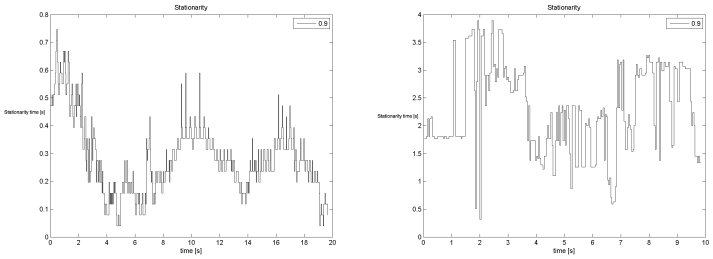

(a) Stationarity time in road crossing (b) Stationarity time in tunnel

Figure 51: Stationarity time in various scenarios

- In road crossing scenario the mean of the different subscenarios is 0.22 s, being the maximum value 0.44 s and the minimum 0.14 s. An example of one experiment is showed in Fig. 51 (a).

- In the rest of the scenarios the mean is 1.45 s, being the maximum value 2.58 s in a traffic congestion scenario and the minimum value 0.77 s in tunnel scenario. Fig. 51 (b) shows an example in tunnel scenario.

To sum up, we can say that when the cars are driving in opposite direction the stationarity time is smaller than when they are driving in the same direction.

Table 5: Stationarity time in various scenarios

Scenarios	**Mean [s]**
Road Crossing: Area rural	0.15
Road Crossing: suburban	0.44
Road Crossing: urban - single lane	0.14
Road Crossing: urban - multiple lanes	0.16
General LOS obstruction	1.44
Merging lanes	0.77
Traffic congestion: Slow traffic	1.27
Traffic congestion: Approaching traffic jam	1.66
In-tunnel	0.97
Bridge	2.58

7.2.8 Time-varying cluster parameters in various scenarios

Table 6 shows the time-varying cluster parameters for each scenario, where we could draw some remarks from it. In annex 10.2 it is possible to find the average and maximum values for the different time-varying cluster parameters and also some plots of this parameters over the time.

The average of the first parameter, number of clusters, is between 1 and 4. Being the scenarios of the highway or rural areas which have the least multipath contributions. By contrast, urban and in-tunnel scenarios are more affected by the multipath propagation. Cluster extension in delay is larger when the environment is rich in diffuse components, as in urban and in-tunnel scenarios. Cluster extension in Doppler is larger depending on the speed of the cars, as in highway situations, and as in urban scenarios it depends also of influence of multipath components.

Table 6: Time-varying cluster parameters in various scenarios

Scenarios	$\bar{N_c}$	$\bar{S_{\tau,1st}}[ns]$	$\bar{S_{v,1st}}[Hz]$
Road Crossing: Area rural	1	24.26	96.61
Road Crossing: suburban	2	43.55	130.86
Road Crossing: urban - single lane	2	74.93	173.28
Road Crossing: urban - multiple lanes	4	79.44	164.14
General LOS obstruction	2	31.67	186.81
Merging lanes	1	35.53	149.01
Traffic congestion: Slow traffic	2	54.65	180.72
Traffic congestion: Approaching traffic jam	2	51.56	168.14
In-tunnel	4	110.40	185.31
Bridge	2	45.63	184.26

8 Conclusions

In this master thesis I have studied the vehicular radio channel. Vehicle-to-vehicle communications are becoming importance in the recent years due to their potential to improve traffic safety.

I carried out an extensive and meticulous research on various aspects related to the characterization of the radio channel. In this work I have been able to fully characterize some of the key channel parameters, which can be further used by researchers developing vehicular channel models. Furthermore, I have not only characterized the mean values of these parameters, but also took into account the non-stationarity nature of the channel and described their time-varying behavior.

I used the vehicular channel data collected in the DRIVEWAY'09 radio measurement campaign, where impulse responses for various scenarios were recorded. The scenarios were chosen such that common risky traffic situations were represented, such as traffic jams, street intersections, driving in-tunnel, etc.

The time-varying channel parameters investigated in this master thesis are:

- rms delay and Doppler spreads,
- stationarity time, and
- identification of scattering objects causing relevant multipath components.

The rms delay and Doppler spreads are important, since they have to be taken into account when designing a system in order to avoid inter-symbol- and inter-carrier-interference. We observed that these parameters are larger in environments where there are lot of objects causing multipath components, as in urban areas and inside tunnels. The maximum rms delay spread is observed *inside tunnels*, where the walls and the ventilation system of the tunnel are the relevant scattering objects.

The stationarity time is the time for which we suppose that the observed fading process is stationary, i.e. the statistical properties within this stationarity time remain constant. We evaluated the stationary time by applying an already established method [add reference] based on a distance metric, the collinearity. The average stationarity time is larger in scenarios where cars drive in the same direction and its value is around 1.5 s. On the contrary, when the cars drive in opposite directions, the mean stationarity time is around 0.5 s.

The third time-varying parameter studied in this master thesis is the identification of objects causing relevant multipath components. After discarding the visual inspection of the power delay profile because of the non rigourousty of the methodology, I proceeded analyzing the local scattering function. By doing so, a new component is taken into account for the characterization, the Doppler shift, which introduces more accuracy in the scatterer identification. Each scattering contribution is represented by a peak in the Doppler-delay plane with a limited extension in both domains. All the multipath components corresponding to the same scatterer have the same statistical properties and can be grouped in clusters in this Doppler-delay plane. Further more, these clusters move in the plane in time, therefore I used a time-varying cluster detection algorithm for detecting the multipath components.

Different time-varying cluster parameters were calculated for the measurement data set. The mean number of detected clusters is between 1 and 5, depending on the selected scenario. We have also noticed that the clusters have an ellipsoid shape, being the delay the shortest axes.

Finally, the cluster extension is influenced basically by the speed of the cars, and the presence and strength of the diffuse components.

Vehicular communications are still being investigated by several research groups in the world. The work done in this master thesis aims to contribute in the time-varying characterization of some very important channel parameters which could be further used, for example, in channel modeling or system design and testing.

9 Outlook

With this master thesis we set up a framework for scatterers identification based on cluster detection. As part of the work, two main time-varying cluster parameters have been investigated: (i) Number of clusters, and (ii) cluster extension. However, this can be further extended by analyzing other parameters such as velocity of the clusters. Based on this parametrization, a simple mathematical cluster-based model can be established for the local scattering function.

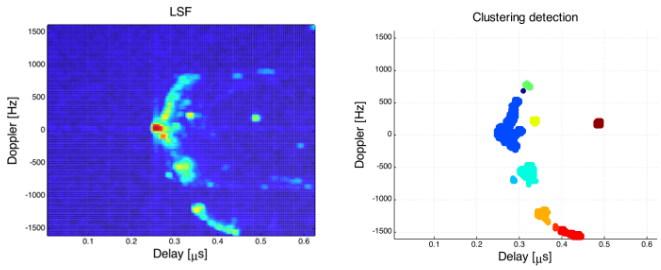

Figure 52: LSF and cluster detection

Furthermore, although the results obtained by the selected cluster detection algorithm are quite accurate, when two clusters are very close to each other, it can happen that they are indistinguishable, as seen in Fig. 52. In these cases, as it was proposed in [24], by implementing the cluster detection algorithm in an iterative way, one should be able to overcome this problem.

10 Annex

10.1 Time-varying channel parameters

10.1.1 Road crossing: Open area rural

Table 7: Mean values of the time-varying channel parameters for scenario 2.1.

Parameters	σ_τ [ns]	τ_{exc} [ns] 10 dB	τ_{exc} [ns] 20 dB	σ_ν [Hz]	ν_{exc} [Hz] 10 dB	ν_{exc} [Hz] 20 dB
Meas 1:	4.96	12.07	12.07	3.42	7.89	7.89
Meas 2:	23.5	19.35	96.9	134.63	75.79	258.79
Meas 3:	48.43	118.04	169.74	57.2	163.57	239.57

Table 8: Maximum values of the time-varying channel parameters for scenario 2.1.

Parameters	σ_τ [ns]	τ_{exc} [ns] 10 dB	τ_{exc} [ns] 20 dB	σ_ν [Hz]	ν_{exc} [Hz] 10 dB	ν_{exc} [Hz] 20 dB
Meas 1:	61.2	145.83	145.83	20.43	50.86	50.86
Meas 2:	59.69	75	491.67	321.27	127.16	381.47
Meas 3:	93.02	295.83	387.5	190.89	610.35	635.78

Table 9: Overall values for scenario 2.1

Parameters	σ_τ [ns]	τ_{exc} [ns] 10 dB	τ_{exc} [ns] 20 dB	σ_ν [Hz]	ν_{exc} [Hz] 10 dB	ν_{exc} [Hz] 20 dB
Mean:	25.63	49.82	92.9	65.08	82.42	168.75
Max:	93.02	295.83	491.67	321.27	610.35	635.78

Table 10: Stationartiy time for scenario2.1

Stationarity	mean	min
Meas 1:	0.15	0.08
Meas 2:	0.24	0.16
Meas 3:	0.06	0.04
Total:	0.15	0.04

10.1.2 Road crossing: Suburban

Table 11: Mean values of the time-varying channel parameters for scenario 2.2 .

Para-	σ_τ	τ_{exc} [ns]		σ_ν	ν_{exc} [Hz]	
meters	[ns]	10 dB	20 dB	[Hz]	10 dB	20 dB
Meas 1:	17.06	17.88	77.37	131.26	81.03	365.34
Meas 2:	18.46	28.53	94.18	99.9	81.83	437.79
Meas 3:	11.14	17.78	55.19	54.09	77.39	192.08
Meas 4:	14.98	20.1	70.84	116.23	82.56	195.23
Meas 5:	13.1	19.08	66.27	73.82	78.91	198.31
Meas 6:	15.62	22.3	73.02	83.53	84.86	186.18
Meas 7:	17.59	15	59.31	94.9	107.29	231.82
Meas 8:	16.59	26.59	76.82	79.58	91.55	195.75
Meas 9:	37.31	38.99	108.67	57.02	73.62	210.55
Meas 10:	23.01	19.29	101.38	104.61	92.72	258.74
Meas 11:	26.05	37.89	142.43	23.64	65.11	113.61

Table 12: Maximum values of the time-varying channel parameters for scenario 2.2 .

Para-	σ_τ	τ_{exc} [ns]		σ_ν	ν_{exc} [Hz]	
meters	[ns]	10 dB	20 dB	[Hz]	10 dB	20 dB
Meas 1:	62.29	145.83	158.33	368.15	228.88	2746.58
Meas 2:	55.3	141.67	241.67	284.3	279.74	2924.6
Meas 3:	62.45	141.67	150	226.34	228.88	330.61
Meas 4:	67.37	150	150	338.71	203.45	330.61
Meas 5:	64.15	145.83	266.67	303.29	254.31	381.47
Meas 6:	66.79	145.83	166.67	302.28	228.88	305.18
Meas 7:	61.08	83.33	191.67	296.47	305.18	406.9
Meas 8:	65.95	150	308.33	285.16	228.88	279.74
Meas 9:	141.83	258.33	1337.5	264.95	152.59	432.33
Meas 10:	52.21	70.83	391.67	238.61	152.59	457.76
Meas 11:	84.7	345.83	612.5	32.68	101.73	254.31

Table 13: Overall values for scenario 2.2

Para-	σ_τ	τ_{exc} [ns]		σ_ν	ν_{exc} [Hz]	
meters	[ns]	10 dB	20 dB	[Hz]	10 dB	20 dB
Mean:	19.17	23.95	84.13	83.51	83.35	235.04
Max:	141.83	345.83	1337.5	368.15	305.18	2924.6

Table 14: Stationartiy time for scenario 2.2

Stationarity	mean	min
Meas 1:	0.26	0.04
Meas 2:	0.24	0.04
Meas 3:	0.24	0.04
Meas 4:	0.25	0.04
Meas 5:	0.27	0.04
Meas 6:	0.26	0.04
Meas 7:	0.24	0.04
Meas 8:	0.22	0.04
Meas 9:	0.13	0.04
Meas 10:	0.17	0.04
Meas 11:	2.54	0.08
Total:	0.44	0.04

10.1.3 Road crossing: Urban - single lane

Table 15: Mean values of the time-varying channel parameters for scenario 2.3 .

Para-meters	σ_τ [ns]	τ_{exc} [ns] 10 dB	τ_{exc} [ns] 20 dB	σ_ν [Hz]	ν_{exc} [Hz] 10 dB	ν_{exc} [Hz] 20 dB
Meas 1:	43.47	113.68	190.17	95.84	181.28	394.29
Meas 2:	43.36	68.39	149.9	209.95	146.12	1026.43
Meas 3:	44.07	80.83	179.38	158.87	179.13	734.33
Meas 4:	33.08	54.02	164.7	125.14	132.65	911.15
Meas 5:	28.15	66.45	132.65	138.06	128.99	867.31

Table 16: Maximum values of the time-varying channel parameters for scenario 2.3 .

Para-meters	σ_τ [ns]	τ_{exc} [ns] 10 dB	τ_{exc} [ns] 20 dB	σ_ν [Hz]	ν_{exc} [Hz] 10 dB	ν_{exc} [Hz] 20 dB
Meas 1:	153.14	229.17	375	594.78	2721.15	2721.15
Meas 2:	65.13	220.83	345.83	452.32	381.47	2873.74
Meas 3:	70.39	233.33	341.67	404.1	432.33	2950.03
Meas 4:	75.19	204.17	491.67	438.88	356.04	3229.78
Meas 5:	58.75	154.17	341.67	473.01	381.47	3229.78

Table 17: Overall values for scenario 2.3

Para-meters	σ_τ [ns]	τ_{exc} [ns] 10 dB	τ_{exc} [ns] 20 dB	σ_ν [Hz]	ν_{exc} [Hz] 10 dB	ν_{exc} [Hz] 20 dB
Mean:	38.43	76.67	163.36	145.57	153.63	786.7
Max:	153.14	233.33	491.67	594.78	2721.15	3229.78

Table 18: Stationartiy time for scenario 2.3

Stationarity	mean	min
Meas 1:	0.14	0.04
Meas 2:	0.15	0.04
Meas 3:	0.14	0.04
Meas 4:	0.14	0.04
Meas 5:	0.12	0.04
Total:	0.14	0.04

10.1.4 Road crossing: Urban - multiple lanes

Table 19: Mean values of the time-varying channel parameters for scenario 2.4 .

Para-meters	σ_τ [ns]	τ_{exc} [ns] 10 dB	τ_{exc} [ns] 20 dB	σ_ν [Hz]	ν_{exc} [Hz] 10 dB	ν_{exc} [Hz] 20 dB
Meas 1:	59.04	137.3	253.45	75.98	128.55	391.4
Meas 2:	64.16	119.7	254.23	83.11	203.14	319.99
Meas 3:	55.3	124.86	274.34	43.45	99.35	205.52
Meas 4:	36.29	130.76	135.01	23.02	66.46	66.46
Meas 5:	52.4	83.13	232.2	146.08	132.55	650.53

Table 20: Maximum values of the time-varying channel parameters for scenario 2.4 .

Para-meters	σ_τ [ns]	τ_{exc} [ns] 10 dB	τ_{exc} [ns] 20 dB	σ_ν [Hz]	ν_{exc} [Hz] 10 dB	ν_{exc} [Hz] 20 dB
Meas 1:	104.5	437.5	504.17	337.62	457.76	1932.78
Meas 2:	115.6	370.83	620.83	285.28	381.47	839.23
Meas 3:	91.59	320.83	537.5	110.61	406.9	457.76
Meas 4:	70.99	341.67	341.67	28.24	101.73	101.73
Meas 5:	120.26	358.33	783.33	498.79	305.18	3229.78

Table 21: Overall values for scenario 2.4

Para-meters	σ_τ [ns]	τ_{exc} [ns] 10 dB	τ_{exc} [ns] 20 dB	σ_ν [Hz]	ν_{exc} [Hz] 10 dB	ν_{exc} [Hz] 20 dB
Mean:	53.44	119.15	229.85	74.33	126.01	326.78
Max:	120.26	437.5	783.33	498.79	457.76	3229.78

Table 22: Stationartiy time for scenario 2.4

Stationarity	mean	min
Meas 1:	0.09	0.04
Meas 2:	0.17	0.04
Meas 3:	0.13	0.04
Meas 4:	0.2	0.08
Meas 5:	0.22	0.04
Total:	0.16	0.04

10.1.5 General LOS obstructed

Table 23: Mean values of the time-varying channel parameters for scenario 3.1 .

Para-meters	σ_τ [ns]	τ_{exc} [ns]		σ_ν [Hz]	ν_{exc} [Hz]	
		10 dB	20 dB		10 dB	20 dB
Meas 1:	98.21	220.85	544.07	67.09	185.95	259.7
Meas 2:	38.45	26.47	209.73	78.48	95.21	447.9
Meas 3:	40.48	84.42	207.18	108.39	269.37	394.59
Meas 4:	35.95	15.05	135.7	56.81	68.87	279.03
Meas 5:	7.44	21.2	39.48	23.44	70.39	73.45
Meas 6:	3.75	11.63	12.26	10.91	28.02	28.02
Meas 7:	34.1	20.73	167.32	36.66	73.65	251.06
Meas 8:	21.15	17.6	103.75	28.61	69.58	184.22
Meas 9:	36.38	16.77	125.32	65.31	65.82	194.91
Meas 10:	46.22	29.25	227.22	33.5	85.86	210.57
Meas 11:	36.3	14.83	146.57	46.1	72.12	347.9
Meas 12:	75.8	193.55	197.35	67.01	141.09	141.09

Table 24: Maximum values of the time-varying channel parameters for scenario 3.1 .

Para-meters	σ_τ [ns]	τ_{exc} [ns]		σ_ν [Hz]	ν_{exc} [Hz]	
		10 dB	20 dB		10 dB	20 dB
Meas 1:	517.69	2129.17	2129.17	541.48	1627.6	1653.04
Meas 2:	79.05	112.5	625	262.2	813.8	1525.88
Meas 3:	138.34	445.83	625	453.74	1118.98	1398.72
Meas 4:	75.95	41.67	283.33	121.59	76.29	1042.68
Meas 5:	24.93	83.33	87.5	27.77	101.73	127.16
Meas 6:	5.93	25	29.17	24.52	76.29	76.29
Meas 7:	152.13	112.5	1425	153.75	254.31	1093.55
Meas 8:	41.1	54.17	208.33	51.93	101.73	356.04
Meas 9:	124.42	50	208.33	153.25	76.29	966.39
Meas 10:	69.07	229.17	425	127.78	178.02	1017.25
Meas 11:	99.07	54.17	583.33	149.08	76.29	1322.43
Meas 12:	290.09	662.5	662.5	316.08	686.65	686.65

Table 25: Overall values for scenario 3.1

Parameters	σ_τ [ns]	τ_{exc} [ns] 10 dB	τ_{exc} [ns] 20 dB	σ_ν [Hz]	ν_{exc} [Hz] 10 dB	ν_{exc} [Hz] 20 dB
Mean:	39.52	56.03	176.33	51.86	102.16	234.37
Max:	517.69	2129.17	2129.17	541.48	1627.6	1653.04

Table 26: Stationartiy time for scenario 3.1

Stationarity	mean	min
Meas 1:	1.64	0.12
Meas 2:	0.59	0.08
Meas 3:	1.12	0.04
Meas 4:	1.03	0.51
Meas 5:	1.04	0.08
Meas 6:	0.83	0.12
Meas 7:	0.84	0.08
Meas 8:	3.06	0.35
Meas 9:	1.64	0.71
Meas 10:	2.51	0.08
Meas 11:	2.76	0.83
Meas 12:	0.23	0.04
Total:	1.44	0.04

10.1.6 Merging lanes

Table 27: Mean values of the time-varying channel parameters for scenario 4.1 .

Para-meters	σ_τ [ns]	τ_{exc} [ns] 10 dB	20 dB	σ_ν [Hz]	ν_{exc} [Hz] 10 dB	20 dB
Meas 1:	12.57	28.08	55.53	37.85	44.02	224.48
Meas 2:	13.18	13.93	69.2	50.06	63.96	247.53
Meas 3:	18.55	13.05	49.15	211	68.44	162.03
Meas 4:	13.53	14.1	44.1	62.3	65.55	165.27
Meas 5:	14.04	12.98	42.44	67.71	61.32	315.35
Meas 6:	16.48	11.29	34.77	78.17	51.14	167.72
Meas 7:	28.51	15.83	112.09	67.31	57.63	443.01
Meas 8:	10.96	18.72	58.69	36.6	85.99	157.61

Table 28: Maximum values of the time-varying channel parameters for scenario 4.1 .

Para-meters	σ_τ [ns]	τ_{exc} [ns] 10 dB	20 dB	σ_ν [Hz]	ν_{exc} [Hz] 10 dB	20 dB
Meas 1:	37.81	95.83	120.83	174.26	203.45	966.39
Meas 2:	28.53	45.83	287.5	177.76	279.74	1042.68
Meas 3:	33.3	25	254.17	308.68	534.06	1525.88
Meas 4:	22.06	33.33	83.33	147.38	279.74	305.18
Meas 5:	32.46	41.67	116.67	263.66	203.45	1068.12
Meas 6:	35.47	50	79.17	346.64	127.16	1093.55
Meas 7:	111.53	83.33	645.83	258.39	101.73	1144.41
Meas 8:	69.43	162.5	200	470.62	1118.98	1220.7

Table 29: Overall values for scenario 4.1

Para-meters	σ_τ [ns]	τ_{exc} [ns] 10 dB	20 dB	σ_ν [Hz]	ν_{exc} [Hz] 10 dB	20 dB
Mean:	15.98	16	58.25	76.37	62.26	235.38
Max:	111.53	162.5	645.83	470.62	1118.98	1525.88

Table 30: Stationartiy time for scenario 4.1

Stationarity	mean	min
Meas 1:	0.13	0.04
Meas 2:	0.95	0.04
Meas 3:	0.75	0.04
Meas 4:	1.28	0.04
Meas 5:	0.93	0.04
Meas 6:	0.91	0.04
Meas 7:	1.09	0.35
Meas 8:	0.13	0.04
Total:	0.77	0.04

10.1.7 Traffic congestion: Slow traffic

Table 31: Mean values of the time-varying channel parameters for scenario 5.1 .

Parameters	σ_τ [ns]	τ_{exc} [ns] 10 dB	τ_{exc} [ns] 20 dB	σ_ν [Hz]	ν_{exc} [Hz] 10 dB	ν_{exc} [Hz] 20 dB
Meas 1:	8.32	25.43	35.62	25.75	61.75	63.99
Meas 2:	10.35	16.4	69.98	26.19	69.78	92.77
Meas 3:	34.73	27.42	231.9	50.67	107.73	279.85
Meas 4:	6.32	16.95	36.92	77.22	221.76	251.67
Meas 5:	20.51	13.93	57.53	29.14	69.99	184.53
Meas 6:	51.67	21.6	277.58	41.19	123.39	229.9
Meas 7:	26.63	28.62	109.28	135.61	68.97	176.9
Meas 8:	19.88	22.42	104.22	57.9	93.18	209.86
Meas 9:	33.53	39.03	171.98	36.5	91.15	224
Meas 10:	21.53	28.17	131.35	34.07	98.47	149.33
Meas 11:	17.27	14.42	68.95	118.57	65.41	198.47

Table 32: Maximum values of the time-varying channel parameters for scenario 5.1 .

Parameters	σ_τ [ns]	τ_{exc} [ns] 10 dB	τ_{exc} [ns] 20 dB	σ_ν [Hz]	ν_{exc} [Hz] 10 dB	ν_{exc} [Hz] 20 dB
Meas 1:	128.81	375	375	202.42	483.19	483.19
Meas 2:	39.62	112.5	287.5	338.82	940.96	940.96
Meas 3:	143.56	120.83	750	228.68	686.65	864.66
Meas 4:	60.11	58.33	337.5	121.11	330.61	330.61
Meas 5:	24.39	20.83	141.67	46.23	76.29	254.31
Meas 6:	133.42	120.83	987.5	51.72	228.88	279.74
Meas 7:	45.94	112.5	229.17	229.76	76.29	279.74
Meas 8:	47.29	116.67	291.67	187.68	432.33	559.49
Meas 9:	51.49	129.17	270.83	47.38	178.02	330.61
Meas 10:	93.41	133.33	683.33	74.47	305.18	330.61
Meas 11:	78.7	45.83	908.33	288.85	76.29	1042.68

Table 33: Overall values for scenario 5.1

Parameters	σ_τ [ns]	τ_{exc} [ns] 10 dB	τ_{exc} [ns] 20 dB	σ_ν [Hz]	ν_{exc} [Hz] 10 dB	ν_{exc} [Hz] 20 dB
Mean:	22.79	23.13	117.76	57.53	97.42	187.39
Max:	143.56	375	987.5	338.82	940.96	1042.68

Table 34: Stationartiy time for scenario 5.1

Stationarity	mean	min
Meas 1:	0.39	0.12
Meas 2:	0.32	0.16
Meas 3:	0.18	0.08
Meas 4:	0.1	0.08
Meas 5:	3.41	1.34
Meas 6:	4.6	1.77
Meas 7:	2.66	0.24
Meas 8:	0.4	0.12
Meas 9:	1.21	0.43
Meas 10:	0.53	0.2
Meas 11:	0.17	0.08
Total:	1.27	0.08

10.1.8 Traffic congestion: Approaching traffic jam

Table 35: Mean values of the time-varying channel parameters for scenario 5.2 .

Para-meters	σ_τ [ns]	τ_{exc} [ns]		σ_ν [Hz]	ν_{exc} [Hz]	
		10 dB	20 dB		10 dB	20 dB
Meas 1:	9.22	17.32	43.85	47.4	77.57	151.98
Meas 2:	15.71	21.94	86.16	41.75	91.3	223.59
Meas 3:	12.84	12.47	64.25	54.63	60.37	191.13
Meas 4:	12.31	14.86	57.13	69.29	69.89	198.52
Meas 5:	16.56	10.84	39.19	28.62	60.07	127.46
Meas 6:	18.27	14.68	70.83	29.13	65.82	208.84
Meas 7:	15.14	24.61	77.51	23.31	62.66	90.38

Table 36: Maximum values of the time-varying channel parameters for scenario 5.2 .

Para-meters	σ_τ [ns]	τ_{exc} [ns]		σ_ν [Hz]	ν_{exc} [Hz]	
		10 dB	20 dB		10 dB	20 dB
Meas 1:	35.42	129.17	212.5	249.71	356.04	432.33
Meas 2:	75.06	241.67	762.5	90.92	330.61	457.76
Meas 3:	66.92	37.5	283.33	272.17	127.16	788.37
Meas 4:	29.13	29.17	125	190.54	101.73	457.76
Meas 5:	22.52	20.83	91.67	58.8	76.29	228.88
Meas 6:	24.06	25	133.33	36.68	76.29	330.61
Meas 7:	49.97	112.5	133.33	39.7	101.73	228.88

Table 37: Overall values for scenario 5.2

Para-meters	σ_τ [ns]	τ_{exc} [ns]		σ_ν [Hz]	ν_{exc} [Hz]	
		10 dB	20 dB		10 dB	20 dB
Mean:	14.29	16.67	62.7	42.02	69.67	170.27
Max:	75.06	241.67	762.5	272.17	356.04	788.37

Table 38: Stationartiy time for scenario 5.2

Stationarity	mean	min
Meas 1:	0.23	0.04
Meas 2:	0.23	0.08
Meas 3:	0.34	0.04
Meas 4:	0.26	0.08
Meas 5:	8.48	0.31
Meas 6:	1.14	0.47
Meas 7:	0.97	0.04
Total:	1.66	0.04

10.1.9 In-tunnel

Table 39: Mean values of the time-varying channel parameters for scenario 6.1 .

Parameters	σ_τ [ns]	τ_{exc} [ns] 10 dB	τ_{exc} [ns] 20 dB	σ_ν [Hz]	ν_{exc} [Hz] 10 dB	ν_{exc} [Hz] 20 dB
Meas 1:	79.2	73	289.3	114.12	76.6	373.54
Meas 2:	68.79	64.53	262.5	107.05	110.68	432.13
Meas 3:	54.87	40.68	256.32	90.24	74.97	656.23
Meas 4:	45.46	36.72	149.95	132.14	78.74	742.49
Meas 5:	75.29	33.33	175.3	166.44	78.33	1103.01
Meas 6:	74.51	42.63	273.03	121.13	77.21	549.32
Meas 7:	53.72	95.18	291.2	46.72	100.4	288.59

Table 40: Maximum values of the time-varying channel parameters for scenario 6.1 .

Parameters	σ_τ [ns]	τ_{exc} [ns] 10 dB	τ_{exc} [ns] 20 dB	σ_ν [Hz]	ν_{exc} [Hz] 10 dB	ν_{exc} [Hz] 20 dB
Meas 1:	109.46	262.5	500	294.39	940.96	1042.68
Meas 2:	99.27	300	533.33	358.5	940.96	1449.58
Meas 3:	95.78	108.33	841.67	297.77	76.29	2085.37
Meas 4:	82.13	145.83	537.5	220.81	203.45	1678.47
Meas 5:	129.6	416.67	983.33	331.73	1068.12	2085.37
Meas 6:	107.33	379.17	687.5	280.02	152.59	1246.13
Meas 7:	75.38	216.67	508.33	334.16	1068.12	1195.27

Table 41: Overall values for scenario 6.1

Parameters	σ_τ [ns]	τ_{exc} [ns] 10 dB	τ_{exc} [ns] 20 dB	σ_ν [Hz]	ν_{exc} [Hz] 10 dB	ν_{exc} [Hz] 20 dB
Mean:	64.55	55.15	242.51	111.12	85.28	592.19
Max:	129.6	416.67	983.33	358.5	1068.12	2085.37

Table 42: Stationartiy time for scenario 6.1

Stationarity	mean	min
Meas 1:	1.05	0.31
Meas 2:	0.59	0.08
Meas 3:	0.23	0.12
Meas 4:	0.53	0.04
Meas 5:	1.92	0.31
Meas 6:	2.19	0.63
Meas 7:	0.29	0.12
Total:	0.97	0.04

10.1.10 Bridge

Table 43: Mean values of the time-varying channel parameters for scenario 6.2 .

Para-	σ_τ	τ_{exc} [ns]		σ_ν	ν_{exc} [Hz]	
meters	[ns]	10 dB	20 dB	[Hz]	10 dB	20 dB
Meas 1:	165.61	48.87	748.83	228.68	283.3	1091.11
Meas 2:	39.63	14.02	148.77	97.13	74.46	514.93
Meas 3:	54.26	14.5	125.6	86.13	86.52	542.65

Table 44: Maximum values of the time-varying channel parameters for scenario 6.2 .

Para-	σ_τ	τ_{exc} [ns]		σ_ν	ν_{exc} [Hz]	
meters	[ns]	10 dB	20 dB	[Hz]	10 dB	20 dB
Meas 1:	626.28	912.5	2129.17	786.8	1042.68	3229.78
Meas 2:	71.41	25	454.17	161.64	76.29	1042.68
Meas 3:	134.81	108.33	1020.83	319.43	1042.68	1118.98

Table 45: Overall values for scenario 6.2

Para-	σ_τ	τ_{exc} [ns]		σ_ν	ν_{exc} [Hz]	
meters	[ns]	10 dB	20 dB	[Hz]	10 dB	20 dB
Mean:	86.5	25.8	341.07	137.31	148.09	716.23
Max:	626.28	912.5	2129.17	786.8	1042.68	3229.78

Table 46: Stationartiy time for scenario 6.2

Stationarity	mean	min
Meas 1:	2.27	0.79
Meas 2:	0.68	0.31
Meas 3:	4.78	0.12
Total:	2.58	0.12

10.2 Time-varying cluster parameters

10.2.1 Road crossing: Open Area Rural

Table 47: Mean of the number of clusters

	$\bar{N}_c$	$maxN_c$	$minN_c$
Experiment1	0.396	4	0
Experiment2	1.428	3	1
Experiment3	1.812	9	0
Total scenario	1.212	9	0

Table 48: Mean of spread in delay and Doppler domain of the first detected cluster

	$\bar{S_{\tau,1st}}$	$\bar{S_{v,1st}}$	$maxS_{\tau,1st}$	$min\tau, 1st$	$maxv, 1st$	$minv, 1st$
Experiment1	4.2	24.821	29.1667	0	127.1566	0
Experiment2	55.4	189.9211	100	25	279.7445	101.7253
Experiment3	13.1667	75.0732	58.3333	0	330.6071	0
Total scenario	24.2556	96.6051	100	0	330.6071	0

Table 49: Mean of spread in delay and Doppler domain of the rest of clusters

	$\bar{S_{\tau,rest}}$	$\bar{S_{v,rest}}$	$maxS_{\tau,rest}$	$min\tau, rest$	$maxv, rest$	$minv, rest$
Experiment1	11.5	65.1042	20.8333	4.1667	101.7253	25.4313
Experiment2	12.279	71.4774	20.8333	4.1667	127.1566	25.4313
Experiment3	15.6228	97.5677	50	4.1667	305.1758	25.4313
Total scenario	13.1339	78.0498	50	4.1667	305.1758	25.4313

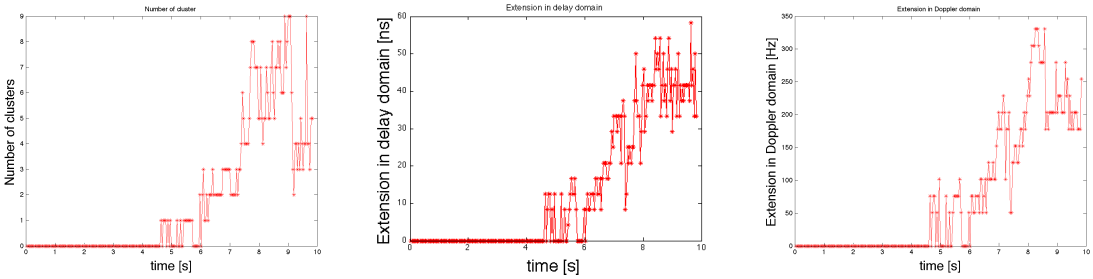

(a) Number of clusters (b) Extension in delay domain (c) Extension in Doppler domain

Figure 53: Time-varying cluster parameters for experiment 3

10.2.2 Road crossing: suburban

Table 50: Mean of the number of clusters

	$\bar{N}_c$	$maxN_c$	$minN_c$
Experiment1	1.514	8	0
Experiment2	1.858	8	0
Experiment3	1.766	7	0
Experiment4	1.6	8	0
Experiment5	1.682	8	0
Experiment6	1.704	6	0
Experiment7	1.834	7	0
Experiment8	1.796	7	0
Experiment9	1.506	7	0
Experiment10	15.06	7	0
Experiment11	15.06	7	0
Total scenario	4.1255	8	0

Table 51: Mean of spread in delay and Doppler domain of the first detected cluster

	$\bar{S}_{\tau,1st}$	$\bar{S}_{v,1st}$	$maxS_{\tau,1st}$	$min\tau, 1st$	$maxv, 1st$	$minv, 1st$
Experiment1	36.0083	119.7815	245.8333	0	356.0384	0
Experiment2	48.85	153.8086	262.5	0	356.0384	0
Experiment3	40.6	135.0403	254.1667	0	356.0384	0
Experiment4	37.8	145.4163	237.5	0	330.6071	0
Experiment5	37.85	124.3591	254.1667	0	356.0384	0
Experiment6	42.925	149.2818	195.8333	0	330.6071	0
Experiment7	64.6917	157.369	279.1667	0	356.0384	0
Experiment8	46.3083	150.7568	241.6667	0	330.6071	0
Experiment9	32.7417	104.0649	175	0	330.6071	0
Experiment10	327.4167	1040.6494	175	0	330.6071	0
Experiment11	327.4167	1040.6494	175	0	330.6071	0
Total scenario	94.7826	301.9252	279.1667	0	356.0384	0

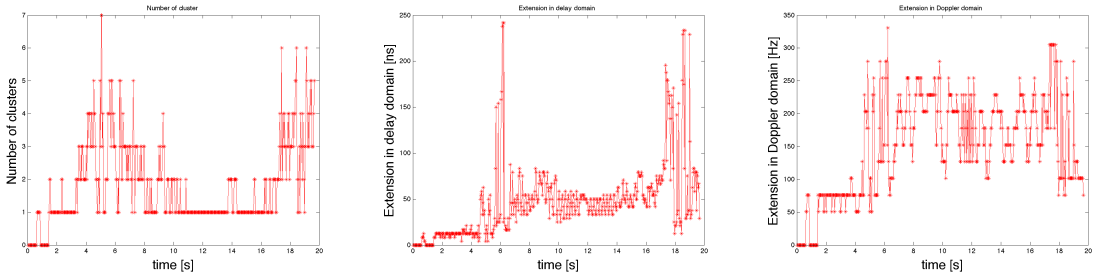

(a) Number of clusters (b) Extension in delay domain (c) Extension in Doppler domain

Figure 54: Time-varying cluster parameters for experiment 8

Table 52: Mean of spread in delay and Doppler domain of the rest of clusters

	$\bar{S}_{\tau,rest}$	$\bar{S}_{v,rest}$	$maxS_{\tau,rest}$	$min\tau, rest$	$maxv, rest$	$minv, rest$
Experiment1	25.4991	91.9898	125	4.1667	254.3132	25.4313
Experiment2	23.3117	90.4161	179.1667	4.1667	305.1758	25.4313
Experiment3	23.4719	90.1896	179.1667	4.1667	305.1758	25.4313
Experiment4	24.0347	94.2702	191.6667	4.1667	305.1758	25.4313
Experiment5	23.8404	93.2918	191.6667	4.1667	305.1758	25.4313
Experiment6	23.8971	94.4853	191.6667	4.1667	305.1758	25.4313
Experiment7	23.0495	93.0557	191.6667	4.1667	305.1758	25.4313
Experiment8	23.7876	95.4622	204.1667	4.1667	330.6071	25.4313
Experiment9	23.3355	94.1826	204.1667	4.1667	330.6071	25.4313
Experiment10	23.3355	94.1826	204.1667	0	330.6071	0
Experiment11	23.3355	94.1826	204.1667	0	330.6071	0
Total scenario	23.7181	93.2462	204.1667	0	330.6071	0

10.2.3 Road crossing: urban- single lane

Table 53: Mean of the number of clusters

	$\bar{N}_c$	$maxN_c$	$minN_c$
Experiment1	1.644	10	0
Experiment2	2.176	9	0
Experiment3	2.136	8	0
Experiment4	2.608	9	1
Experiment5	2.248	7	1
Total scenario	2.1624	10	0

Table 54: Mean of spread in delay and Doppler domain of the first detected cluster

	$\bar{S}_{\tau,1st}$	$\bar{S}_{v,1st}$	$maxS_{\tau,1st}$	$min\tau, 1st$	$maxv, 1st$	$minv, 1st$
Experiment1	63.8167	119.8324	250	0	483.195	0
Experiment2	61.0833	167.5415	254.1667	0	483.195	0
Experiment3	67.9	163.3708	254.1667	0	559.4889	0
Experiment4	85.6833	191.2435	237.5	4.1667	432.3324	50.8626
Experiment5	96.1833	224.4059	212.5	4.1667	534.0576	50.8626
Total scenario	74.9333	173.2788	254.1667	0	559.4889	0

Table 55: Mean of spread in delay and Doppler domain of the rest of clusters

	$\bar{S}_{\tau,rest}$	$\bar{S}_{v,rest}$	$maxS_{\tau,rest}$	$min\tau, rest$	$maxv, rest$	$minv, rest$
Experiment1	19.4844	78.7639	158.3333	4.1667	254.3132	25.4313
Experiment2	21.7755	82.5559	183.3333	4.1667	356.0384	25.4313
Experiment3	21.8837	83.1572	204.1667	4.1667	457.7637	25.4313
Experiment4	22.797	89.2343	204.1667	4.1667	457.7637	25.4313
Experiment5	22.6622	90.837	204.1667	4.1667	534.0576	25.4313
Total scenario	21.7206	84.9097	204.1667	4.1667	534.0576	25.4313

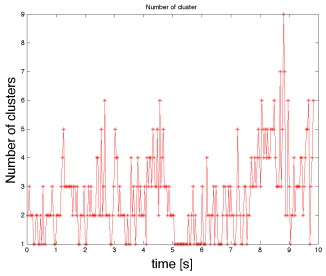

(a) Number of clusters

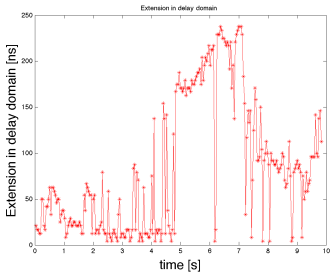

(b) Extension in delay domain

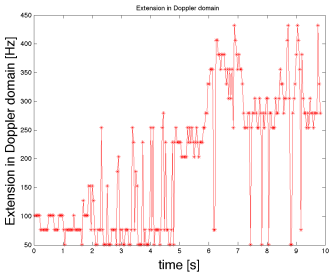

(c) Extension in Doppler domain

Figure 55: Time-varying cluster parameters for experiment 4

10.2.4 General LOS obstruction

Table 56: Mean of the number of clusters

	$\bar{N_c}$	$maxN_c$	$minN_c$
Experiment1	4.7	12	1
Experiment2	3.132	11	1
Experiment3	5.444	17	1
Experiment4	1.704	4	1
Experiment5	1.4	4	1
Experiment6	0.956	1	0
Experiment7	2.144	13	1
Experiment8	1.896	7	1
Experiment9	1.568	3	1
Experiment10	2.948	5	1
Experiment11	1.268	3	1
Experiment12	1.932	4	1
Total scenario	2.4243	17	0

Table 57: Mean of spread in delay and Doppler domain of the first detected cluster

	$\bar{S_{\tau,1st}}$	$\bar{S_{v,1st}}$	$maxS_{\tau,1st}$	$min\tau, 1st$	$maxv, 1st$	$minv, 1st$
Experiment1	36.4	200.5005	45.8333	29.1667	305.1758	127.1566
Experiment2	37.6833	227.6611	58.3333	25	559.4889	101.7253
Experiment3	44.0667	294.5964	79.1667	25	1042.6839	101.7253
Experiment4	27.6167	170.4915	50	20.8333	228.8818	101.7253
Experiment5	34.8167	173.9502	45.8333	20.8333	254.3132	101.7253
Experiment6	17.8	89.8234	33.3333	0	203.4505	0
Experiment7	31.7167	204.1626	87.5	20.8333	381.4697	101.7253
Experiment58	30.3833	185.0382	79.1667	20.8333	356.0384	101.7253
Experiment59	30.0667	170.2881	37.5	20.8333	279.7445	101.7253
Experiment10	28.0167	193.278	45.8333	20.8333	279.7445	101.7253
Experiment11	23.8833	187.8866	33.3333	20.8333	254.3132	101.7253
Experiment12	37.6833	144.043	58.3333	16.6667	305.1758	76.2939
Total scenario	31.6778	186.81	87.5	0	1042.6839	0

Table 58: Mean of spread in delay and Doppler domain of the rest of clusters

	$\bar{S}_{\tau,rest}$	$\bar{S}_{\upsilon,rest}$	$maxS_{\tau,rest}$	$min\tau, rest$	$max\upsilon, rest$	$min\upsilon, rest$
Experiment1	13.0895	77.4474	29.1667	4.1667	178.0192	25.4313
Experiment2	13.3082	78.0719	70.8333	4.1667	254.3132	25.4313
Experiment3	14.3353	81.1823	91.6667	4.1667	534.0576	25.4313
Experiment4	14.0856	80.3967	91.6667	4.1667	534.0576	25.4313
Experiment5	14.0504	80.3865	91.6667	4.1667	534.0576	25.4313
Experiment6	14.0504	80.3865	91.6667	0	534.0576	0
Experiment7	13.9448	80.3376	91.6667	4.1667	534.0576	25.4313
Experiment8	13.8607	80.1587	91.6667	4.1667	534.0576	25.4313
Experiment9	13.8127	80.0817	91.6667	4.1667	534.0576	25.4313
Experiment10	13.785	80.1549	91.6667	4.1667	534.0576	25.4313
Experiment11	13.7453	80.0597	91.6667	4.1667	534.0576	25.4313
Experiment12	13.9897	80.4722	91.6667	4.1667	534.0576	25.4313
Total scenario	13.8381	79.928	91.6667	0	534.0576	0

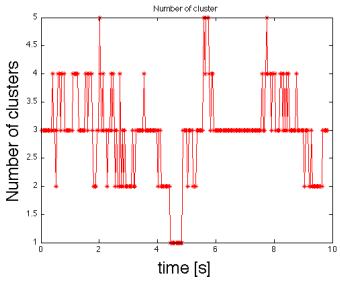

(a) Number of clusters

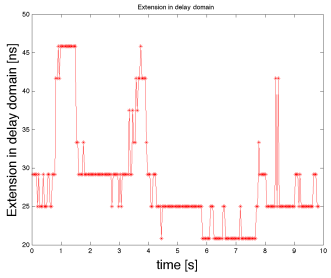

(b) Extension in delay domain

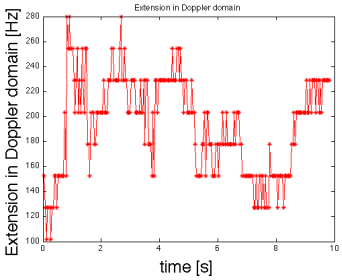

(c) Extension in Doppler domain

Figure 56: Time-varying cluster parameters for experiment 10

10.2.5 Merging lanes

Table 59: Mean of the number of clusters

	$\bar{N_c}$	$maxN_c$	$minN_c$
Experiment1	1.192	3	1
Experiment2	0.456	5	0
Experiment3	0.894	3	0
Experiment4	0.842	4	0
Experiment5	0.752	3	0
Experiment6	0.834	6	0
Experiment7	0.744	5	0
Experiment8	1.568	4	1
Experiment9	2.808	4	0
Total scenario	1.1211	6	0

Table 60: Mean of spread in delay and Doppler domain of the first detected cluster

	$\bar{S_{\tau,1st}}$	$\bar{S_{v,1st}}$	$maxS_{\tau,1st}$	$min\tau, 1st$	$maxv, 1st$	$minv, 1st$
Experiment1	48.0083	199.0255	62.5	4.1667	330.6071	76.2939
Experiment2	6.1167	45.5729	54.1667	0	635.7829	0
Experiment3	30.475	130.717	62.5	0	356.0384	0
Experiment4	29.4667	139.4653	66.6667	0	864.6647	0
Experiment5	29.8167	128.0212	62.5	0	381.4697	0
Experiment6	29.6917	140.9403	62.5	0	406.901	0
Experiment7	21.9583	113.0676	62.5	0	406.901	0
Experiment8	45.0917	134.6334	79.1667	25	254.3132	101.7253
Experiment9	79.1167	309.6517	66.6667	0	254.3132	0
Total scenario	35.5269	149.0106	79.1667	0	864.6647	0

Table 61: Mean of spread in delay and Doppler domain of the rest of clusters

	$\bar{S_{\tau,rest}}$	$\bar{S_{v,rest}}$	$maxS_{\tau,rest}$	$min\tau, rest$	$maxv, rest$	$minv, rest$
Experiment1	10.7818	49.8139	50	4.1667	152.5879	25.4313
Experiment2	13.0233	73.0997	50	4.1667	305.1758	25.4313
Experiment3	12.8286	75.3824	50	4.1667	305.1758	25.4313
Experiment4	13.145	80.4669	50	4.1667	432.3324	25.4313
Experiment5	13.1924	81.0482	50	4.1667	432.3324	25.4313
Experiment6	14.4531	85.7645	58.3333	4.1667	432.3324	25.4313
Experiment7	15.4055	88.7815	58.3333	4.1667	432.3324	25.4313
Experiment8	14.8801	84.2717	58.3333	4.1667	432.3324	25.4313
Experiment9	14.9507	84.4922	58.3333	0	432.3324	0
Total scenario	13.6289	78.1246	58.3333	0	432.3324	0

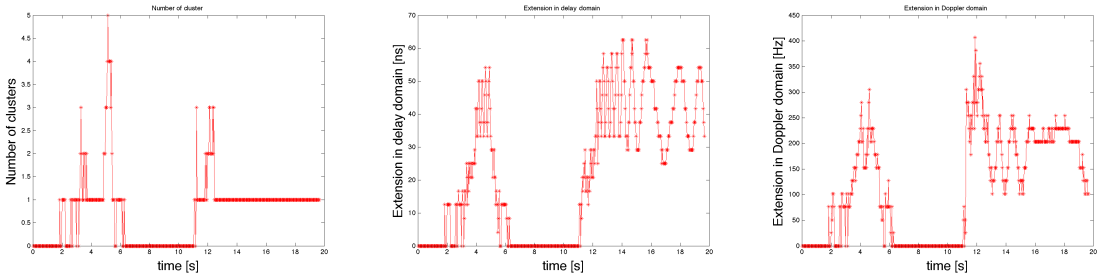

(a) Number of clusters (b) Extension in delay domain (c) Extension in Doppler domain

Figure 57: Time-varying cluster parameters for experiment 7

10.2.6 Traffic congestion: Slow traffic

Table 62: Mean of the number of clusters

	$\bar{N_c}$	$maxN_c$	$minN_c$
Experiment1	1.436	3	1
Experiment2	1.06	2	1
Experiment3	4.844	8	2
Experiment4	1.576	3	1
Experiment5	1.776	6	1
Experiment6	2.744	6	1
Experiment7	2.032	5	1
Experiment8	1.12	2	1
Experiment9	1.256	3	1
Experiment10	1.332	3	1
Experiment11	3.32	12	1
Total scenario	2.0451	12	1

Table 63: Mean of spread in delay and Doppler domain of the first detected cluster

	$\bar{S_{\tau,1st}}$	$\bar{S_{v,1st}}$	$maxS_{\tau,1st}$	$min\tau, 1st$	$maxv, 1st$	$minv, 1st$
Experiment1	43.7333	150.9603	83.3333	20.8333	228.8818	76.2939
Experiment2	45.5833	181.2744	70.8333	25	254.3132	101.7253
Experiment3	84.8833	204.6712	195.8333	45.8333	330.6071	101.7253
Experiment4	68.0667	188.2935	183.3333	25	279.7445	101.7253
Experiment5	55.6167	192.9728	116.6667	25	330.6071	101.7253
Experiment6	78.7833	189.3107	158.3333	33.3333	279.7445	101.7253
Experiment7	48.2333	191.04	112.5	25	279.7445	101.7253
Experiment8	44.2167	180.2572	75	29.1667	279.7445	101.7253
Experiment9	36.45	158.2845	58.3333	25	432.3324	76.2939
Experiment10	41.9333	162.8621	79.1667	16.6667	254.3132	76.2939
Experiment11	53.6667	187.9883	100	25	330.6071	127.1566
Total scenario	54.6515	180.7195	195.8333	16.6667	432.3324	76.2939

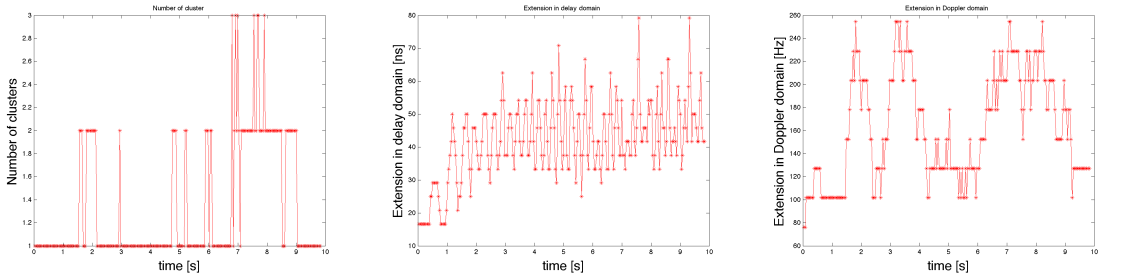

(a) Number of clusters (b) Extension in delay domain (c) Extension in Doppler domain

Figure 58: Time-varying cluster parameters for experiment 10

Table 64: Mean of spread in delay and Doppler domain of the rest of clusters

	$\bar{S}_{\tau,rest}$	$\bar{S}_{v,rest}$	$maxS_{\tau,rest}$	$min\tau, rest$	$maxv, rest$	$minv, rest$
Experiment1	12.6515	71.2077	25	4.1667	101.7253	50.8626
Experiment2	11.8333	69.1732	25	4.1667	101.7253	50.8626
Experiment3	21.4319	88.6349	112.5	4.1667	305.1758	25.4313
Experiment4	20.5894	86.5492	112.5	4.1667	305.1758	25.4313
Experiment5	19.6776	86.4558	112.5	4.1667	305.1758	25.4313
Experiment6	18.3669	84.1694	112.5	4.1667	305.1758	25.4313
Experiment7	18.0752	84.3628	112.5	4.1667	305.1758	25.4313
Experiment8	17.9683	84.1317	112.5	4.1667	305.1758	25.4313
Experiment9	17.8345	84.1924	112.5	4.1667	305.1758	25.4313
Experiment10	17.776	83.8181	112.5	4.1667	305.1758	25.4313
Experiment11	16.887	82.4682	112.5	4.1667	305.1758	25.4313
Total scenario	17.5538	82.2876	112.5	4.1667	305.1758	25.4313

10.2.7 Traffic congestion: Approaching traffic jam

Table 65: Mean of the number of clusters

	$\bar{N}_c$	$maxN_c$	$minN_c$
Experiment1	1.724	4	1
Experiment2	2.108	6	1
Experiment3	2.002	6	1
Experiment4	1.17	3	1
Experiment5	1.036	2	1
Experiment6	1.234	3	1
Experiment7	1.844	4	1
Total scenario	1.5883	6	1

Table 66: Mean of spread in delay and Doppler domain of the first detected cluster

	$\bar{S}_{\tau,1st}$	$\bar{S}_{v,1st}$	$maxS_{\tau,1st}$	$min\tau, 1st$	$maxv, 1st$	$minv, 1st$
Experiment1	59.3917	187.6831	100	25	279.7445	101.7253
Experiment2	48.4167	166.7786	95.8333	20.8333	330.6071	101.7253
Experiment3	52.0583	187.6322	141.6667	25	305.1758	101.7253
Experiment4	48.925	177.2054	91.6667	25	254.3132	101.7253
Experiment5	38.75	139.4653	70.8333	25	254.3132	101.7253
Experiment6	50.1583	157.369	79.1667	29.1667	254.3132	101.7253
Experiment7	63.2583	160.8276	108.3333	16.6667	279.7445	76.2939
Total scenario	51.5655	168.1373	141.6667	16.6667	330.6071	76.2939

10.2.8 In-tunnel

Table 67: Mean of spread in delay and Doppler domain of the rest of clusters

	$S_{\tau,rest}$	$S_{v,rest}$	$maxS_{\tau,rest}$	$min\tau, rest$	$maxv, rest$	$minv, rest$
Experiment1	12.741	76.364	37.5	4.1667	178.0192	25.4313
Experiment2	12.55	74.3526	41.6667	4.1667	178.0192	25.4313
Experiment3	15.4707	80.5983	100	4.1667	305.1758	25.4313
Experiment4	15.2085	79.9487	100	4.1667	305.1758	25.4313
Experiment5	15.1134	79.6213	100	4.1667	305.1758	25.4313
Experiment6	14.9013	78.6228	100	4.1667	305.1758	25.4313
Experiment7	14.8928	77.726	100	4.1667	305.1758	25.4313
Total scenario	14.4111	78.1762	100	4.1667	305.1758	25.4313

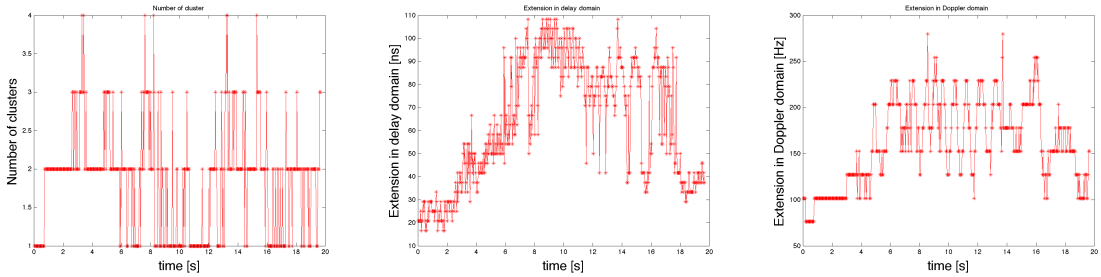

(a) Number of clusters (b) Extension in delay domain (c) Extension in Doppler domain

Figure 59: Time-varying cluster parameters for experiment 7

Table 68: Mean of the number of clusters

	$\bar{N}_c$	$maxN_c$	$minN_c$
Experiment1	5.216	10	2
Experiment2	4.688	14	1
Experiment3	2.66	7	1
Experiment4	1.824	4	1
Experiment5	1.536	3	1
Experiment6	4.528	11	1
Experiment7	4.244	8	1
Total scenario	3.528	14	1

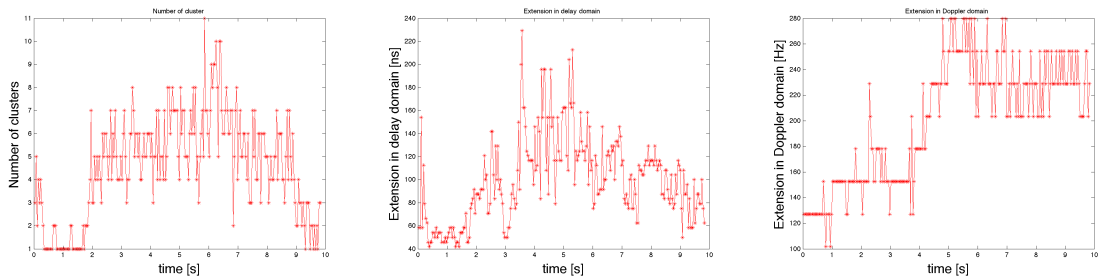

(a) Number of clusters (b) Extension in delay domain (c) Extension in Doppler domain

Figure 60: Time-varying cluster parameters for experiment 7

Table 69: Mean of spread in delay and Doppler domain of the first detected cluster

	$\bar{S}_{\tau,1st}$	$\bar{S}_{v,1st}$	$maxS_{\tau,1st}$	$min\tau, 1st$	$maxv, 1st$	$minv, 1st$
Experiment1	129.5667	159.5052	250	58.3333	254.3132	101.7253
Experiment2	115	170.1864	275	45.8333	254.3132	101.7253
Experiment3	98.3167	192.159	170.8333	58.3333	254.3132	127.1566
Experiment4	69	205.7902	104.1667	29.1667	305.1758	127.1566
Experiment5	67.1	184.8348	100	37.5	254.3132	101.7253
Experiment6	99.5833	199.7884	229.1667	41.6667	279.7445	101.7253
Experiment7	194.25	184.9365	350	4.1667	254.3132	50.8626
Total scenario	110.4024	185.3144	350	4.1667	305.1758	50.8626

Table 70: Mean of spread in delay and Doppler domain of the rest of clusters

	$\bar{S}_{\tau,rest}$	$\bar{S}_{v,rest}$	$maxS_{\tau,rest}$	$min\tau, rest$	$maxv, rest$	$minv, rest$
Experiment1	20.1106	79.3312	87.5	4.1667	127.1566	25.4313
Experiment2	19.0777	77.8118	87.5	4.1667	203.4505	25.4313
Experiment3	18.1682	76.581	87.5	4.1667	203.4505	25.4313
Experiment4	17.8198	76.8813	87.5	4.1667	203.4505	25.4313
Experiment5	17.5833	76.8245	87.5	4.1667	203.4505	25.4313
Experiment6	18.1735	76.695	104.1667	4.1667	203.4505	25.4313
Experiment7	18.7411	76.3572	308.3333	4.1667	203.4505	25.4313
Total scenario	18.5249	77.2117	308.3333	4.1667	203.4505	25.4313

10.2.9 Bridge

Table 71: Mean of the number of clusters

	$\bar{N}_c$	$maxN_c$	$minN_c$
Experiment1	1.996	4	1
Experiment2	1.848	4	1
Experiment3	1.708	14	1
Total scenario	1.8507	14	1

Table 72: Mean of spread in delay and Doppler domain of the first detected cluster

	$\bar{S}_{\tau,1st}$	$\bar{S}_{v,1st}$	$maxS_{\tau,1st}$	$min\tau, 1st$	$maxv, 1st$	$minv, 1st$
Experiment1	49.4333	198.0591	70.8333	25	279.7445	101.7253
Experiment2	42.6167	196.9401	79.1667	25	254.3132	101.7253
Experiment3	44.8417	157.7759	95.8333	25	305.1758	101.7253
Total scenario	45.6306	184.2584	95.8333	25	305.1758	101.7253

Table 73: Mean of spread in delay and Doppler domain of the rest of clusters

	$\bar{S}_{\tau,rest}$	$\bar{S}_{v,rest}$	$maxS_{\tau,rest}$	$min\tau, rest$	$maxv, rest$	$minv, rest$
Experiment1	13.4167	80.8716	20.8333	4.1667	127.1566	25.4313
Experiment2	12.7345	76.0187	20.8333	4.1667	127.1566	25.4313
Experiment3	12.5306	74.2993	29.1667	4.1667	152.5879	25.4313
Total scenario	12.8939	77.0632	29.1667	4.1667	152.5879	25.4313

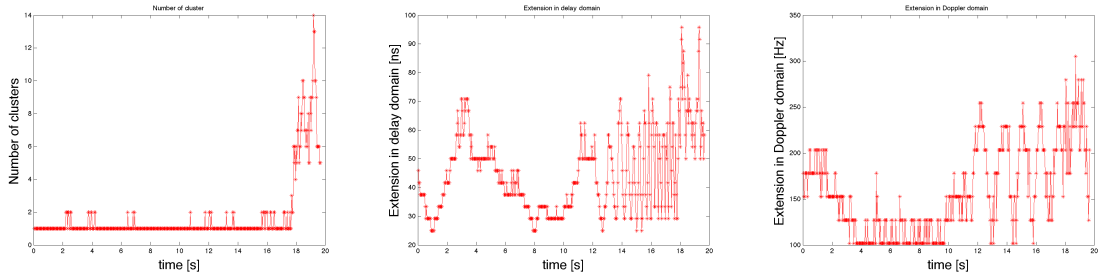

(a) Number of clusters (b) Extension in delay domain (c) Extension in Doppler domain

Figure 61: Time-varying cluster parameters for experiment 4

References

[1] D. C. et al, "Peformance of ieee 802.11a in vehicular contexts," 2007.

[2] E. A. et al, "Accuracy and efficiency in simulating vanets,"

[3] Y. Toor and P. Mühlethaler, "Vehicle ad hoc netweorks: Applications and related technical issues," 2008.

[4] D. Jiang and L. Delgrossi, "Ieee 802.11p: Towards an international standard for wireless access in vehicular environments," 2008.

[5] A. Festag, A. Hessler, R. Baldessari, L.Le, W. Zhang, and D. Westhoff, "Vehicle-to-vehicle and road-side sensor communication for enhanced road safety,"

[6] O. Klemp, A. Thiel, A. Paier, L. Bernadó, J. Karedal, and A. Kwoczek, "In-situ vehicular antenna integration and design aspects for vehicle-to-vehicle communications," 2009.

[7] A. Paier, J. Karedal, N.Czink, H. Hofstetter, C. Dumard, T. Zemen, F.Tufvesson, C. F. Mecklenbräuker, and A. F. Molisch, "First results from car-to-car and car-to-infrastructure radio channel measurements at 5.2 ghz," 2007.

[8] A. Paier, J. Karedal, N. Czink, H. Hofstetter, C. Dumard, T. Zemen, F. Tufvesson, A. F. Molisch, and C. F. Mecklenbräuker, "Characterization of vehicle-to-vehicle radio channels from measurements at 5.2 ghz," 2007.

[9] A. Paier, T. Zemen, L. Bernadó, G. Matz, J. Karedal, N. Czink, C. Dumard, F. Tufvesson, A. F. Molisch, and C. F. Mecklenbräuker, "Non-wssus vehicular channel characterization in highway and urban scenarios at 5.2 ghz using the local scattering function," 2008.

[10] L. Bernadó, T. Zemen, A. Paier, J. Karedal, and B. Fleury, "Parametrization of the local scattering function estimator for vehicular-to-vehicular channels," *Procceedings IEEE VTC Fall 2009*, 2009.

[11] A. Paier, L.Bernadó, J. Karedal, O. Klemp, A. Kwoczek, F. Tufvesson, A. Thiel, Y. Zhou, N. Czink, T. Zemen, A. F. Molisch, and C. F. Mecklenbräuker, "Overview of vehicle-to-vehicle radio channel measurements for collision avoidance applications," 2009.

[12] G. Acosta-Marum and M. Ingram, "Six time- and frequency- selective empirical channel models for vehicular wireless lan's," 2007.

[13] G. Acosta-Marum and M. I. K. Tokunda, "Measured joint doppler-delay power profiles for vehicle-to-vehicle communications at 2.4 ghz," 2004.

[14] I. Sen and S. Matolak, "Vehicle-to-vehicle channel models for the 5-ghz band," 2007.

[15] P. Paschalidis, M. Wisotzki, A. Kortke, W. Keusgen, and M. Peter, "A wideband channel sounder for car-to-car radio channel measurements at 5.7 ghz and results for an urban scenario," 2008.

[16] L. Cheng, B. Henty, F. Bai, and D. Stancil, "Higway and rural propagation channel modeling for vehicle-to-vehicle communications at 5.9 ghz," 2008.

[17] L. Bernadó, T. Zemen, A. Paier, G. Matz, J. Karedal, N. Czink, C. Dumard, F. Tufvesson, M. Hagenauer, A. F. Molisch, and C. F. Mecklenbräuker, "Non-wssus vehicular channel characterization at 5.2 ghz- spectral divergence and time-variant coherence parameters," 2008.

[18] G. Matz, "On non-wssus wireless fading channels," *IEEE Transactions on Wireless Communications*, 2005.

[19] A. F. Molisch, *Wireless communication*. New York, USA: Cambridge University Press, 2005.

[20] J. Karedal, F. Tufvesson, N. Czink, A. Paier, C. Dumard, T. Zemen, C. F. Mecklenbräuker, and A. F. Molisch, "A geometry-based stochastic mimo model for vehicle-to-vehicle communications," *IEEE Transactions on Wireless Communications*, vol. 8, no. 7, pp. 3646–3657, 2009.

[21] G. Matz, "Doubly underspread non- wssus channels: Analysis and estimation of channel statistics," pp. 190–194, June 2003.

[22] N. Czink, "The random-cluster model – a stochastic mimo channel model for broadband wireless communication systems of the 3rd generation and beyond," 2007.

[23] D. Kim, K. Lee, D. Lee, and K. Lee, "A kernel-based subtractive clustering method," 2004.

[24] M. Ester, H.-P. Kriegel, J. Sander, and X.Xu, "A density-based algorithm for discovering clusters in large spatial databases with noise," *International Conference on Knowledge Discovery and Mining*, 1996.